
Long-term monitoring reveals unprecedented stability of a vent mussel assemblage on the Mid-Atlantic Ridge

Van Audenhaege Loïc ^{1,*}, Matabos Marjolaine ¹, Brind'Amour Anik ², Drugmand Jonathan ^{1,3}, Laes Agathe ⁴, Sarradin Pierre-Marie ¹, Sarrazin Jozee ¹

¹ Univ Brest, CNRS, Ifremer, UMR6197 BEEP, F-29280 Plouzané, France

² DECOD (Ecosystem Dynamics and Sustainability), IFREMER, INRAE, Institut Agro, Nantes, France

³ Université catholique de Louvain, Ecole de biologie, B-1348 Louvain-la-Neuve, Belgique

⁴ Ifremer, REM/RDT/LDCM, F-29280 Plouzané, France

* Corresponding author : Loïc Van Audenhaege, email address : loic.van.audenhaege@ifremer.fr

marjolaine.matabos@ifremer.fr ; anik.brindamour@ifremer.fr ; jonathan.drugmand@uclouvain.be ; agathe.laes@ifremer.fr ; pierre.marie.sarradin@ifremer.fr ; jozee.sarrazin@ifremer.fr

Abstract :

Understanding scales and drivers of ecological variability is essential to a full understanding of ecosystem functioning. At remote deep-sea hydrothermal vents, infra-annual dynamics remain poorly described. This study aims to characterise the factors that drive the dynamics of a vent faunal assemblage dominated by *Bathymodiolus azoricus* mussels from infra-daily to monthly time steps. We analysed a 7-year time series of images and environmental data collected at 1695 m depth at the base of the active Eiffel Tower edifice in the Lucky Strike vent field (Mid-Atlantic Ridge). Using images acquired by the TEMPO ecological module connected to the EMSO-Azores observatory, we assessed the dynamics of key species inhabiting the faunal assemblage in relation to changes in environmental conditions monitored daily.

Our results show that habitat conditions were generally stable over the 7-year period, with small-scale variability related to tidal periodicity and local temperature anomalies. Likewise, the mussel and zoanthid assemblages exhibited remarkable stability. Changes in fluid exposure and substratum instability induced decimetre-scale movements of the mussel assemblage. Microbial mats displayed infra-annual changes characterised by aperiodic growth and decline. Their development patterns could not be entirely attributed to environmental conditions, because other factors, including biotic interactions, appeared to be involved. The crab population preferentially occupied the mussel habitat, but no predation was observed. Scales of variation and driving factors were compared with those governing intertidal zones. The outcomes question the assumption that vent fauna experience extreme and highly variable conditions. On the MAR, mussel assemblages appear to experience relatively stable and mild environmental conditions compared with their coastal counterparts.

Highlights

► The diffuse-flow habitat was highly stable over 7 years. ► The *Bathymodiolus azoricus* mussel assemblage was remarkably stable over 7 years. ► Microbial mats displayed heterogeneous spatio-temporal dynamics. ► The zoanthid assemblage was highly stable. ► Few biotic interactions were observed such as facilitation mechanisms. ► Comparison to intertidal mussel dynamics demonstrates a regime of infrequent disturbance on vent assemblages.

Keywords : Hydrothermal ecology, Ecosystem functioning, Deep-sea observatory, Underwater imagery, *Bathymodiolus azoricus*, Species behaviour, Habitat monitoring, Multidisciplinary research

1. Introduction

Hydrothermal vents result from the emission of superheated fluids that are released on the seafloor through the advection of cold seawater in the oceanic crust where a variety of mixing and reactive processes occur. These fluids are enriched with reduced chemicals that are used by chemoautotrophic organisms to sustain exceptionally dense faunal communities in a generally food-deprived deep sea. A variety of microhabitats are spread along a dilution gradient between hot hydrothermal fluids and cold oxygenated seawater (Jannasch 1985). Despite the presence of environmentally stressful conditions, vent ecosystems sustain luxuriant communities of endemic species, often dominated by large endosymbiotic invertebrates (Tunnicliffe 1991; Childress and Fisher 1992; L veill  et al. 2005). Vent species are distributed according to their nutritional needs as well as their physiological tolerance to environmental conditions (Vismann 1991). Their habitats are characterised by steep centimetre- to metre-scale gradients of physico-chemical conditions that can vary through time due to tidal and hydrodynamic forcing (Johnson et al. 1988a; Chevaldonn  et al. 1991; Le Bris et al. 2006; Podowski et al. 2009; Lee et al. 2015). Biotic interactions also influence the spatial distribution of the vent fauna (Micheli et al. 2002; Mullineaux et al. 2003; Sancho et al. 2005; Lenihan et al. 2008). At longer time scales, succession mechanisms are also controlled by changes in venting activity, habitat modifications and stochastic events (Fustec et al. 1987; Tunnicliffe et al. 1990, 1997; Sarrazin et al. 1997, 2002; Shank et al. 1998; Marcus et al. 2009). Although we are beginning to understand the spatial distribution of vent assemblages, resolving the scales of ecological variability and underlying mechanisms is paramount to reaching a fuller understanding of vent ecosystem functioning (Levin 1992; Wiens et al. 1993).

Discovered in 1993, Lucky Strike (LS) is a basalt-hosted vent field located in the Azores Triple Junction on the slow-spreading Mid-Atlantic Ridge, at a depth of ~1700 m (Langmuir et al. 1993). This large hydrothermal field (~1 km²) lies at the summit of a seamount that harbours a

central fossilised lava lake surrounded by three volcanic cones (Fouquet et al. 1994; Langmuir et al. 1997; Cannat et al. 1999; Figure 1A). More than 20 active hydrothermal sites have been discovered (Von Damm et al. 1998; Charlou et al. 2000; Ondréas et al. 2009; Barreyre et al. 2012), all fed by a unique source (Pester et al. 2012; Chavagnac et al. 2018) fuelled by an axial magmatic chamber (Singh et al. 2006). Differences in hydrothermal fluid composition occur among vent sites due to varying geological settings and permeability of the upflow zone (Charlou et al. 2000; Leleu et al. 2015; Chavagnac et al. 2018). Eiffel Tower (ET), located east of the lava lake, is the most studied hydrothermal edifice of the vent field, and its ecology has been thoroughly investigated for over 20 years (e.g. Sarradin et al. 1999; Desbruyères et al. 2001; Cuvelier et al. 2009, 2011a; b; De Busserolles et al. 2009; Crépeau et al. 2011; Martins et al. 2011; Sarrazin et al. 2015, 2020; Husson et al. 2017; Girard et al. 2020; Figure 1B). This 11 m edifice consists of a massive sulphide deposit of ~452 m² (Girard et al. 2020) surrounded by a peripheral zone extending more than 20 m from the summit (Cuvelier et al. 2009). Hydrothermal activity occurs on the main sulphide tower and at the periphery through focused releases, flanges and diffuse outflows (Cuvelier et al. 2009; Mittelstaedt et al. 2012).

Similar to several edifices of LS, ET diffusion zones are dominated by the symbiont-bearing mussel *Bathymodiolus azoricus* Cosel & Comtet, 1999 and shrimp *Mirocaris fortunata* Martin & Christiansen, 1995 forming two main assemblages: those found in warmer and more variable habitats (5.2-9.5°C) and visually dominated by *M. fortunata* and those visually dominated by *B. azoricus* in colder habitats (4.4-6.1°C; Cuvelier et al. 2011a; Sarrazin et al. 2015, 2020; Husson et al. 2017). The biomass of ET is largely dominated by *B. azoricus* mussels (~90%, Husson et al. 2017), which can thrive in a wide range of trophic niches. For their nutrition, they mostly rely on sulphur and methane-oxidising *Gammaproteobacteria* endosymbionts hosted in their gills (Fiala-Médioni et al. 2002; Duperron et al. 2006). However, they are also able to filter-feed (Riou et al. 2010); this nutritional mode is more common in smaller individuals

(Martins et al. 2008; De Busserolles et al. 2009). *B. azoricus* is considered an engineer species, because the 3D structure of their aggregations provides shelter, feeding grounds and various microhabitats. At ET, over 79 species of macro- and meiofauna composed of grazers, predators and detritivores have been identified in these assemblages (review by Husson et al. 2017). Mussels can be further subdivided into distinct assemblages, corresponding to different microhabitats and various shell sizes (Cuvelier et al. 2009; Sarrazin et al. 2015; Husson et al. 2017). Faunal diversity varies along the mixing gradient between vent fluids and ambient seawater ($\sim 4.4^{\circ}\text{C}$), with higher densities and richness in lower temperature habitats (Sarrazin et al. 2015). Dense colonies of unidentified zoanthid colonise the bare substratum in the periphery of the ET sulphide edifice (Husson et al. 2017; Girard et al. 2020). The most mobile taxa, such as *M. fortunata* shrimp and the crab *Segonzacia mesatlantica* Williams, 1998, occupy a wide range of temperature niches (Husson et al. 2017). Both species occupy the highest level of the trophic network (De Busserolles et al. 2009), either as predators or scavengers. Moreover, *S. mesatlantica* shows territorial behaviour and is occasionally observed feeding on mussels (Matabos et al. 2015). The ichthyofauna consists of a few visiting species (Cuvelier et al. 2009, 2017). To complete the picture, microbial communities form visible mats that cover all kinds of hard substrata including mussel shells (Cuvelier et al. 2009; Crépeau et al. 2011). These microbial mats are dominated by *Gammaproteobacteria* sulphur-oxidisers such as *Beggiatoa* spp. which give them a white filamentous aspect (Crépeau et al. 2011). They are found in low-temperature areas ($< 6^{\circ}\text{C}$, Cuvelier et al. 2011a) that benefit from hydrothermal particles conveyed by bottom currents (Girard et al. 2020). Although the factors explaining the spatial distribution of these assemblages have been identified and niches of dominant species characterised, much less is known about their infra-annual temporal dynamics.

Compared with vent fields located on faster spreading ridges, catastrophic events at LS rarely occur (review in Glover et al. 2010). In fact, only one major seismic event — a dike intrusion

in 2001 — has been recorded (Dziak et al. 2004). At ET, a temporal study based on imagery reported the stability of vent communities and environmental conditions over 14 years and suggested that faunal communities may have reached a climax state (Cuvelier et al. 2011b). Some authors have suggested that in conditions of low environmental stress and relative stability, biotic factors may play a crucial role in the structure of hydrothermal communities (Sarrazin et al. 1997; review in Glover et al. 2010). Negative interactions including predation, larviphagy, physical disturbance, grazing activities (Johnson et al. 1988b; Micheli et al. 2002; Sancho et al. 2005; Lenihan et al. 2008; Marticorena et al. 2021), as well as facilitation (Sarrazin et al. 1997, Mullineaux et al. 2003) influence faunal distribution. However, the absence of long-term, high-frequency observations has restricted our ability to determine the relative roles of biotic and abiotic factors in shaping vent communities (Tunnicliffe et al. 1990; Grelon et al. 2006; Matabos et al. 2015; Cuvelier et al. 2017). The long-term acquisition of high-resolution infra-annual time series of faunal and environmental changes is therefore essential to gain further knowledge on factors driving community dynamics in these ecosystems. The development of deep-sea observatories now offers this possibility (Matabos et al. 2016).

In 2010, after many years of scientific cruises at LS, a multidisciplinary observatory — EMSO-Azores — was installed to monitor the long-term dynamics of physical, chemical and geophysical factors and evaluate their impact on faunal communities (Cannat et al. 2011, 2016). Two Sea Monitoring Nodes (SeaMON) are the energy suppliers and communication relays for a variety of sensors deployed on the seafloor (Figure 1A). Data is acoustically transferred to a surface buoy (BOREL) that ensures the relay between the nodes and an IFREMER SISMER data centre on land via satellite (Blandin et al. 2010). The SeaMON East node is dedicated to ecological studies and includes, among others, the TEMPO ecological observation module (Sarrazin et al. 2007, Figure 1C-D). Equipped with a camera and environmental sensors, TEMPO records high-resolution images as well as physico-chemical conditions (temperature,

dissolved oxygen and iron concentrations) within the field of view of the camera (Figure 2). The area chosen to study long-term vent faunal assemblage dynamics is located at the base of Eiffel Tower and is colonised by a dense *B. azoricus* assemblage.

A pilot study using TEMPO imagery in this area provided the first insights into the day-to-day variations in the mussel assemblage for the 48 days during which the video camera was operational (Sarrazin et al. 2014). Daily observations showed that the assemblage was quite stable, reflecting the relative stability of environmental conditions during this period. *B. azoricus* mussels thrived in habitats with very limited hydrothermal fluid input and significantly influenced by ocean tidal signals (Sarrazin et al. 2014). Temporal variation in species abundance was observed, but — with the exception of *M. fortunata* shrimp — no link could be established with measured environmental factors (Sarrazin et al. 2014; Cuvelier et al. 2017). Although these imagery studies did not indicate a clear tidal influence on LS mussel assemblages, Mat et al. (2020) recently showed that the physiology and behaviour of *B. azoricus* were significantly influenced by these periodic variations. Nevertheless, questions about the processes influencing long-term variations remain. What are the underlying mechanisms acting on mussel assemblage dynamics over a period of several years? Can we observe biological processes such as interactions, settlement, mortality, reproduction? From infra-daily to pluriannual time scales, which environmental drivers explain habitat variability? Can any stochastic events be linked with biological responses? These questions will be addressed by analysing the spatio-temporal variability of biological processes and environmental conditions in the monitored diffuse-flow habitat. Imagery recorded between 2012 and 2019 by the TEMPO biological observatory module at ET will be combined with *in situ* measurements to address the following hypotheses: (H1) local environmental conditions vary at scales of minutes to days, but generally remain stable over a long period of several years; (H2) mussel cover and (H3) microbial mat cover similarly remain stable over a period

of several years; (H4) zoanthid abundance does not vary significantly over long time periods, (H5) the spatial distribution of fauna is linked to particular environmental conditions and/or substratum types and (H6) biotic interactions (e.g. facilitation, predation, competition) have a significant influence on faunal/microbial distribution.

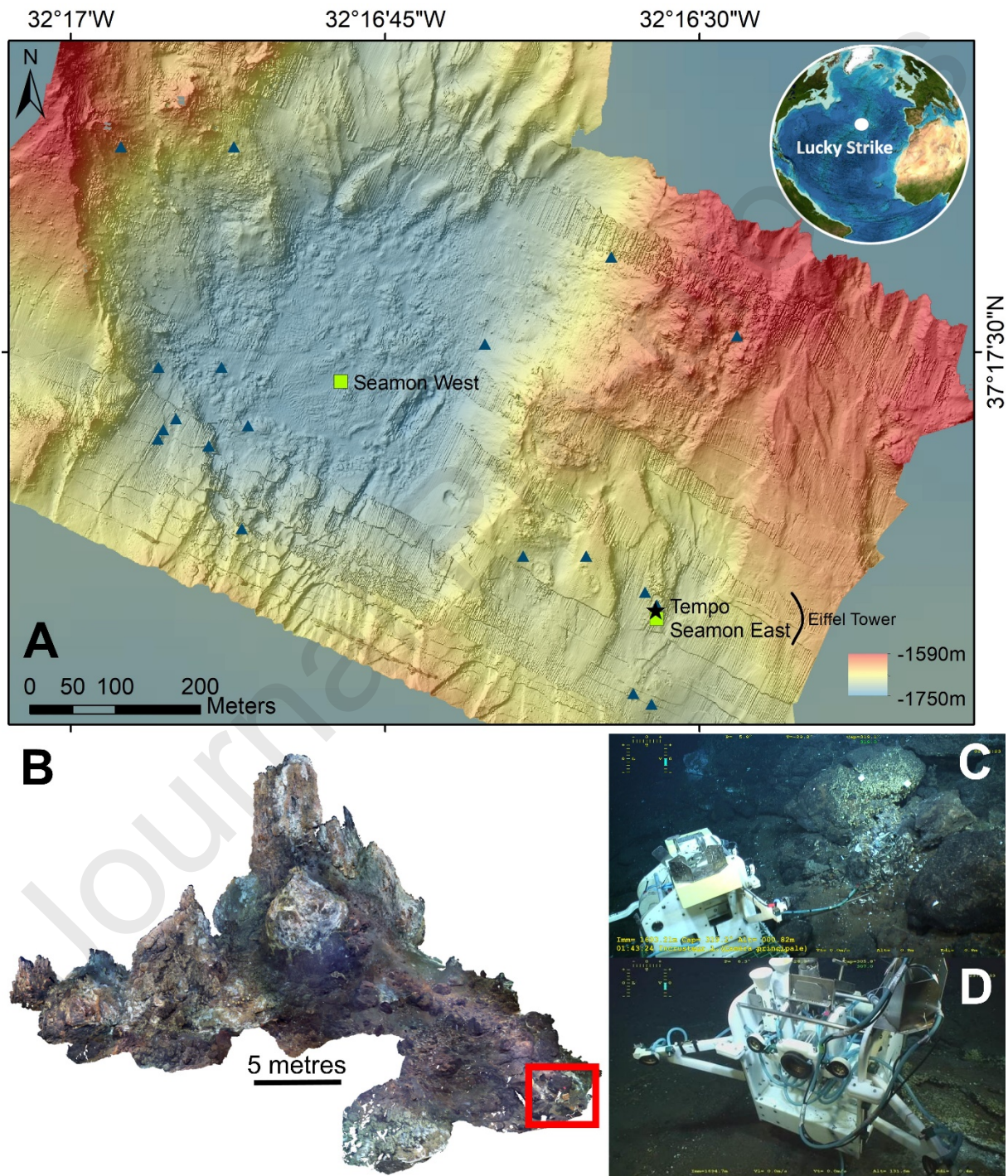


Figure 1. (A) Map of the Lucky Strike vent field (northern Mid-Atlantic Ridge). The colour gradient corresponds to the bathymetry (Ondréas et al. 2009). Active vent sites are indicated with blue triangles. Green squares indicate the location of the SeaMON nodes. The TEMPO ecological module location is shown by a black star. (B) 3D reconstruction of the Eiffel Tower edifice (ET; Matabos and Arnaubec 2015). The red box indicates the monitoring area, located 30 metres away from the summit of ET. (C) Side view of the TEMPO ecological module monitoring a mussel assemblage in a diffuse-flow habitat. The blue cable on the seabed links the CHEMINI iron *in situ* analyser and the sampling inlet deployed in the field of view. (D) Front view of the TEMPO ecological module. The central porthole is the camera. The yellow subtext in Figure 1C & 1D is the submersible's navigation information encrusted in the images and should not be considered by the reader.

2. Materials and methods

2.1. Data acquisition and pre-processing

Since 2010, the TEMPO ecological module (Figure 1B) has been capturing high-resolution daily video sequences of a bathymodiolin mussel assemblage inhabiting a diffuse-flow habitat at the base of the ET sulphide edifice (Sarrazin et al. 2014; Matabos et al. 2015). Two types of images are available depending on the zoom level and two acquisition strategies were adopted as a trade-off between the scientific questions and the limited energy supply. Between 2012 and 2015, zoomed-out videos were acquired four times a day to study the role of tidal oscillations on species behaviour and assemblage dynamics (Cuvelier et al. 2017; Mat et al. 2020). In 2015, we changed our acquisition strategy because we did not observe major changes in species distribution at a daily scale. From then on, zoomed-out sequences were recorded only once a week (2015-2016) and then only once every 10 days (2016-2019). In this study, we only considered zoomed-out sequences. Screenshots were extracted from imagery using FFmpeg libraries.

Every year, TEMPO is recovered and redeployed with an underwater vehicle (i.e. HOV *Nautilie* or ROV *Victor6000*) for maintenance; therefore, its position varies slightly between recording time intervals (hereafter called “period”). In addition, currents may cause slight displacement of the bottom-deployed module. As a result, the image time series does not always capture exactly the same scene, making it challenging to conduct long-term quantitative assessments of

changes in assemblage dynamics. A routine was developed in Python (v.3.7.4) to overlay the different snapshots on a common spatial system (available upon request). This overlay routine is based on the common features between image pairs, selected with a combination of 1) automatic detection by the Speeded-Up Robust Features detection algorithm (SURF; Bay et al. 2006; OpenCV library v.4.1.2.30; Howse 2013) on images pre-processed for contrast enhancement with the OpenCV CLAHE algorithm, and 2) manual annotations using Hugin software (v.2019.2.0; d'Angelo 2005). Finally, a RANSAC regression over distances between paired detection points determined the optimal homography transformation matrix computed for each image, within and among periods (Agarwal et al. 2005; Supplementary Video 1). The dimensions of any object observable in the pictures were averaged to scale the images (0.65 mm/pixel) assuming a 2D and planar field of view (FoV). The surface areas of the different FoVs over time varied from 94.9 to 210.2 dm² among image acquisition periods. After homography transformation, two FoVs representing the area captured in 2012-2015 and 2012-2019 respectively were defined. The FoVs considered for long-term monitoring included a large FoV (78.85 dm², 2012-2015) and a smaller one (35.66 dm², 2012-2019) which was comprised within the 2012-2015 FoV (Figure 2).

The TEMPO ecological module is equipped with an environmental module that measured temperature and oxygen concentrations in the FoV every 15 minutes (Aanderaa Data Instruments Inc., TD 218 3830), and iron concentrations ([Fe(II)+ Fe(III)]) with the CHEMINI chemical analyser every 24 h (12 h for 2018-2019) with 2 to 4 replicates depending on the period (Vuillemin et al. 2009; Laes-Huon et al. 2016; Figure 2, Table 1). For the oxygen optode calibration, salinity was pre-set to 3.5‰ following the manufacturer's recommendations. Moreover, oxygen concentrations were depth-compensated according to the manufacturer's instructions to account for 3.2% of the lower response of the sensing foil per 1000 m depth. Between 2012 and 2015, the *in situ* CHEMINI iron analyser was calibrated daily. Given that

these calibrations were very stable during the whole deployment time, the *in situ* calibration was extended to once a week from 2015 to 2019. The inlet nozzle of the chemical analyser was associated with a MISO temperature probe.

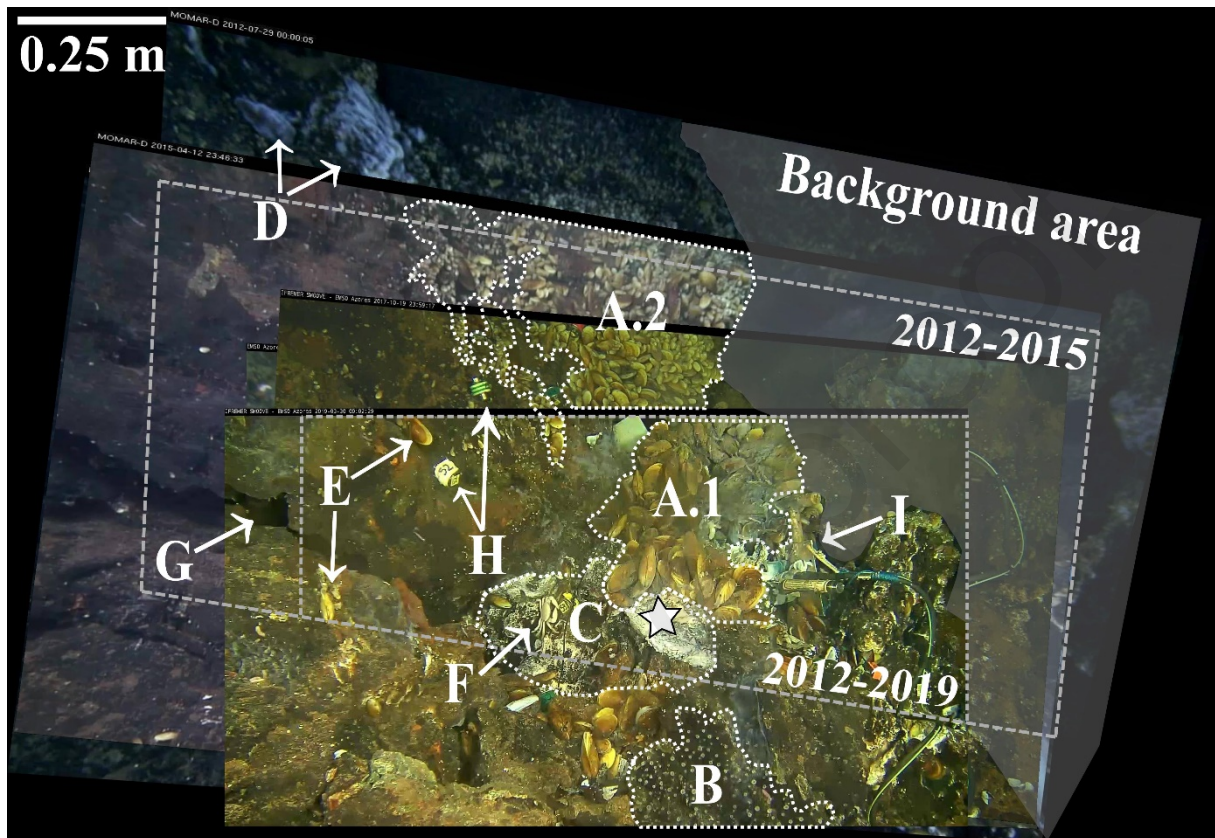


Figure 2. Field of view (FoV) recorded by the TEMPO module and capturing the evolution of a diffuse-flow habitat over 7 years at the base of the Eiffel Tower (ET) edifice (Lucky Strike, Mid-Atlantic Ridge). The white star shows the locations of shimmering water in video sequences. Image overlay was achieved using homography based on a combination of manual and automatic feature detection. Two FoVs are delineated by grey dashed boxes and were determined as the common area for two temporal windows: 2012-2015, comprised in the 2012-2019 window. The grey shaded section represents the background area, parts of that sections in the FOVs were discarded for image analysis. Various elements are delineated in the image. (A) *Bathymodiolus azoricus* mussel assemblage displaying size-based zonation: (A.1) a lower portion with densely packed large mussels and (A.2) an upper portion with sparse patches of small(er) mussels. (B) Patch of zoanthids located on a hard substratum. (C) White material where a small flange was observed growing on the outcrop on the right side of that area. This material extends behind that small outcrop, but it was not visible in the FoV. (D) White filamentous microbial mats. (E) *B. azoricus* individuals for which displacement can be tracked. (F) A *Segonzacia mesatlantica* crab. (G) Crevice in the bare substratum. (H) iButton® probes in titanium casings. They are separated by ~20 cm and tied together with a fine string. (I) TEMPO Environmental module with two temperature probes, a CHEMINI dissolved iron analyser and an optode.

Table 1 – Parameters of (1) environmental data acquired from *in situ* measurements recorded by the TEMPO ecological module (EMSO-Azores observatory) and during yearly visits with a submersible from July 2012 to June 2019, and (2) biological data extracted from images. Sampling frequency may vary among periods of data acquisition. FoV: Field of view. n is the number of measurements for environmental data or images/video sequences for biological data. See Section 2.1 for details on video data acquisition as recorded *in situ*.

(1) Environmental data			
	Variable	Data acquisition parameters	Data analysis
Hydrothermal vent fluid characteristics	Dissolved iron [Fe(II)+ Fe(III)] concentration [μmol/L]	<i>In situ</i> chemical analyser CHEMINI. 1 to 2 measurements per day.	n = 1160 for 2013-2015 and 2016-2019
	Oxygen concentration [μmol/L] and temperature [°C]	Optode. 1 measurement every 15 to 30 min.	n = 186,862 for 2012-2019
	Temperature [°C]	Autonomous probe on the CHEMINI analyser. 1 measurement every 2 to 15 min	n = 286,145 for 2012-2013, 2014-2015, 2016-2019
Background environmental parameters	Turbidity [NTU]	Turbidity sensor on SeaMON East. 1 measurement every 15 min.	n = 168,959 for 2015-2018
	Temperature [°C]	Autonomous probe attached on the LED projectors of TEMPO. 1 measurement every 2 to 15 min.	n = 516,125 for 2012-2014 and 2016-2019
Habitat heterogeneity	Temperature [°C]	iButtons® visible in the TEMPO FoV. 1 measurement every 1-2 hours. Values summarised as	n = 21,988 for 2014-2019 (32 temperature sensors deployed)

Time series plot (for all)

Whittaker-Robinson periodograms (for all)

Time series plot (for all)

Whittaker-Robinson periodograms (for all)

Whittaker-Robinson periodograms

Spatio-temporal empirical orthogonal function (EOF)** analysis

	the average over 1 week centred on the end of the month	(n = 25, p = 99 grid cells) based on monthly linear regressions (R ² , p-value) on iButton® temperatures according to the distance from the warmest recordings (only for iButton®).
Temperature [°C]	<i>In situ</i> submersible probe from an average temperature over 1 minute. Yearly measurements with a submersible in the TEMPO FoV	n = 87 for 2014-2019 except for the 2015 expedition
Dissolved iron [Fe (II)] concentration [μmol/L]	<i>In situ</i> chemical analyser CHEMINI on the submersible. Yearly measurements with a submersible in the TEMPO FoV	n = 77 for 2014-2019
Total sulphide (ΣS=H ₂ S+HS ⁻ +S ²⁻) concentration [μmol/L]	<i>In situ</i> chemical analyser CHEMINI on the submersible. Yearly measurements with a submersible in the TEMPO FoV	n = 99 for 2014-2019

(2) Biological data

Variable	Taxon	Data extraction parameters	Data analyses
Cover	<i>Bathymodiolus azoricus</i>	1 image per month	n = 29 for 2012-2015 Total cover time series & linear regression (R ² , p-value)
			n = 67 for 2012-2019 Maps of mean occurrence* Spatio-temporal empirical orthogonal function (EOF) analysis** (2012-2015: p = 627 grid cells, 2012-2019: p = 253 grid cells)
Microbial mat		1 daily image	n = 93 for 3 months of 2012-2013 Total cover time series
		1 image per 7 days (2015-2016) and 10 days (all other periods)	n = 80 for 2012-2015 Total cover time series Maps of mean occurrence* Spatio-temporal empirical orthogonal functions (EOF) analysis** (2012-2015: p = 627 grid cells, 2012-2019: p = 253)

			n = 170 for 2012-2019	grid cells)
Error of cover annotation	Observer's reproducibility: <i>Bathymodiolus azoricus</i> , microbial mat	3 annotation replicates	n = 8 random images	Coefficient of variation
	Infra-daily variability: Microbial mat	3 annotation of individual patch of microbial mat at different moment within a video (2012-2013)	n = 15 patches	Coefficient of variation
Tracks of individual displacements	<i>Bathymodiolus azoricus</i>	Individual positioning every 6 hours	n = 36 individuals, over 4140 images for 2011-2015	Trajectory of displacement Mann-Whitney U test for trajectory differences
Density (counts)	Zoanthid	Automated detection: daily (2014-2015), weekly (2015-2016), 10 days (2017-2018, 2018-2019) Manual annotation: 3 replicates every 3 months	n = 280 n = 16	Linear regression
	<i>Segonzacia mesatlantica</i>	One image every 6 h for 2012-2015, weekly for 2015-2016, 10 days for 2016-2019	n = 3120	Whittaker-Robinson periodograms for periods of 2012-2015
		One image every 7 (2015-2016) or 10 days (2012-2015, 2016-2019)	n = 119 for 2012-2015 FoV n = 202 for 2012-2019 FoV	Friedman test and Wilcoxon-Nemenyi-McDonald-Thompson post-hoc test
Interactions & predatory activity	<i>Segonzacia mesatlantica</i> & fishes	Video sequences: 4 x 2 min a day in 2012-2015, 5 min/week in 2015-2016, 8 min/10 days in 2016-2019	122.5 h viewed	Observation of interspecific interactions

*Maps of mean occurrence were built by summing the presence (= 1) over the whole time series in each pixel **EOFs are the equivalent of a principal component analysis (PCA) performed on space (each pixel representing a "species") and time (each date represents an "observation/site") matrix for each response variable (biological component or temperature)

Additionally, since 2014, up to four arrays of five autonomous sensors (Thermochron iButton®; $\pm 0.5^\circ\text{C}$) placed in titanium casings tied with a fine string that maintains them up to 20 cm apart, were deployed each year in the FoV to record hourly temperatures within the diffuse-flow habitat (Figure 2, Table 1). iButton® position was annotated monthly in images and a temperature average over a week was assigned to each position. The physico-chemical characterisation of the habitat was done during yearly maintenance cruises with the submersible high-temperature probe and an *in situ* CHEMINI chemical analyser operated by the submersible that measured total sulphide (ΣS ; $\text{H}_2\text{S}+\text{HS}^-+\text{S}^{2-}$) and dissolved iron Fe(II) concentrations from 2014 to 2019. CHEMINI measurements were conducted on each iButton® temperature and at additional points on distinct biological features and substrata (Figure 2). The detection limits were set to three times the standard deviation recorded using a blank solution measurement while on the seafloor. The detection limits for iron and total sulphide concentrations were on average 0.31 and 0.56 $\mu\text{mol/L}$, respectively, and CHEMINI concentrations lower than the dive-specific detection limits were set to 0. For a better understanding of the time series, the temporal coverage of each data type is detailed in Table 1 (see Supplementary Figure 1). Monitoring of background environmental parameters was performed with a turbidity sensor (ECO-BBRTD, WET labs, Inc.) deployed on the SeaMON East station (Figure 1) and by an autonomous probe (MISO; Fornari et al. 1998) placed on the TEMPO module away from hydrothermal activity and measuring ambient seawater temperature.

2.2. Extraction of biological data through image processing

Three dominant visible taxa, including the ecosystem-engineer mussel *B. azoricus*, the crab *S. mesatlantica* and an unidentified zoanthid species, as well as white filamentous microbial mats were studied here (Figure 2). Cover was annotated as polygon features (mussels and mats), and individual organisms (crabs and zoanthids) were annotated as points. All annotations were determined with ImageJ® (Rasband 1997). Coordinates (in pixels) were then transformed in

the new common image system and scaled as defined in Section 2.1 for further comparison over time. Investigating long-term dynamics requires a trade-off between minimising the processing time and maximising the amount of information gained. If possible, the frequency of data extraction was adapted to reduce annotation time (Table 1).

Cover dynamics - Cover dynamics were investigated for *B. azoricus* and microbial mats. As image spatial extents were not identical across all periods, analyses were separated into the two FoVs delimited by masks computed in the homography correction workflow. The poorly visible background area (Figure 2) and the TEMPO environmental module, which partly occupied the FoV (8.85 dm², Figure 2.1), were discarded from analyses. For mussels and microbial mats, the observer's reproducibility (Schoening et al. 2016) was evaluated by replicating three cover annotations of eight random images from which the variation coefficient was determined (Table 1). In addition, movements of mussels or mats that may influence cover variability at short time scales were studied. For mussels, they can be due to changes in mussel shell orientation within a single day (authors' pers. obs.), but we assumed that they do not affect the total surface covered over the long term (Cuvelier et al. 2017). For microbial mats, infra-daily variability may be linked to the flapping movements of the microbial filaments induced by variability in bottom currents. Therefore, 15 randomly chosen patches from three video sequences were annotated on three screenshots taken randomly within the original video sequence (Table 1). The final annotation error was estimated by summing the maximum coefficient of variation of both annotation errors (i.e. observer's reproducibility and infra-daily variability) and set to $\pm 5\%$ for *B. azoricus* cover and $\pm 30\%$ for microbial mat cover.

Mussel cover - Preliminary weekly and daily observations showed *B. azoricus* cover to be stable at the scale of weeks and only changing gradually over time (authors' pers. obs.). Given that these observations were also consistent with previous results at ET (Sarrazin et al. 2014; Cuvelier et al. 2017), we selected a monthly time step to characterise mussel assemblage

dynamics in the present study (Table 1). In addition, *B. azoricus* individuals were tracked to assess the role of mobility on assemblage dynamics using video screenshots from 2011 to 2015 (Table 1). Positions of these mussels were recorded every 6 h and only if they were traceable over more than one image. Three scenarios were possible: individuals were either leaving the assemblage, entering the image FoV from the bare substratum on the left or moving within the assemblage (Figure 2). The final displacement rate was then standardised to the total number of mussels forming the main assemblage.

Microbial mat cover - For microbial mat dynamics, daily annotations were first carried out over a continuous 3-month image series (i.e. 27 July 2012 to 27 October 2012). Daily variability in microbial mat cover was lower than the annotation precision, and growth and decrease occurred progressively over several weeks (Supplementary Figure 2). Therefore, their long-term dynamics were evaluated using the shortest image acquisition time step common to each time series (7 days for 2015-2016 and 10 days for 2012-2015 and 2016-2019, Table 1).

Zoanthid density - Zoanthid assemblage dynamics were investigated for periods of at least 3 months when image quality allowed the quantification of single individuals (Table 1). Regions of interest (ROIs) were delimited to exclude areas with microbial mats that interfered with zoanthid detection. Cnidarian individuals were counted automatically at daily to 10-day intervals (Table 1) using an .IMJ image segmentation routine (ImageJ®; Rasband 1997) involving smoothing and contrast-enhancing filters on the image's green channel. Individuals were isolated by subtracting a period-calibrated threshold value from a binary image. The ImageJ® particle analyser plug-in (Ferreira and Rasband 2012) was then used on resulting images to automate the count of individuals. As suggested by Aron et al. (2013), manual individual counts were replicated three times in images with a 3-month interval to validate the results from the automatic detection (Table 1). Zoanthid abundances were transformed to

density over dm^2 . Temporal trends in the automated and manual detection methods were similar, validating the automated detection workflow.

Individual observations - Individual crabs were counted on all snapshots with support of video sequences for movement detection (Figure 2, Table 1). Their position was recorded using ImageJ®. To investigate preferential substratum occupancy, hydrothermal features, crevices and the TEMPO environmental module were delimited. The area not delimited by polygons was inferred to be “bare substratum”. Predatory activities and interactions with crabs and visiting fishes were investigated by watching the entire sequence of each video at 16x speed. In total, this accounted for 122.5 h of video sequences (Table 1).

2.3. Data analyses

Environmental conditions - Whittaker-Robinson periodograms were used to assess tidal periodicity in environmental parameters. They were performed on the residuals from least-square linear regressions of the environmental time series (i.e. temperature, dissolved oxygen and iron concentrations) to remove any linear trends in the data (Legendre and Legendre 2012; Table 1). Permutations were used to estimate the associated p -values ($n=499$, Legendre 2012). We selected periodogram outputs considering the periods nearest in time to 12.5 h and 25 h corresponding to the semi-diurnal and diurnal tidal signals usually detectable in temperatures collected at LS (Khripounoff et al. 2008; Sarrazin et al. 2014).

Temporal dynamics in biological variables - Dynamics of biological variables were investigated by plotting either the total cover (mussels, microbial mats) or density (zoanthids) computed from annotations over time. Slopes of linear regressions were used to investigate temporal trends in the data. A Shapiro-Wilk test (1965) was performed to verify that the residuals were normally distributed. When this assumption was met and the slope significant, adjusted R^2 was used to assess data dispersion.

Spatio-temporal distribution of *Bathymodiolus azoricus* and microbial mats - The general spatial distribution of mussels and microbial mats over time was investigated by summing up the presence/absence (i.e. 1 and 0) in each pixel individually throughout the time series (Table 1). The mean occurrence of mussels or microbial mats was then estimated over the time series by dividing the total occurrence in each pixel by the total number of images considered in each FoV. This procedure was used to build maps of mean occurrence in each FoV.

To investigate spatio-temporal dynamics within the FoV, each image (i.e. an observation in time) was split over space by dividing the FoV in grid cells of 5 x 5 cm, to which local percentages of cover were assigned based on the presence/absence of mussels or mats in the corresponding pixels (5929 pixels in each grid cell; Table 1). A time x space matrix was constructed and used in subsequent analyses, with each row corresponding to one image (i.e. a vector of grid cells), and each column being a date in the time series. Empirical orthogonal functions (EOFs) were computed on that time x space matrix to highlight the spatial structure of the temporal variability in mussel and microbial mat cover (Preisendorfer and Mobley 1988; review in Hannachi et al. 2007). Similar to a principal component analysis (PCA), an EOF analysis decomposes the signals by determining the set of orthogonal functions that minimise the residual variance in the data. Eigenvectors were computed from the covariance of the time x space matrix and only EOFs explaining at least 10% of the variance were selected. The temporal structure of each biological component was then relayed by drawing each eigenvector over time, by plotting the coordinates of each observation (i.e. image) along the EOF of interest. To characterise the spatial structure of the temporal variability represented by the first EOFs, the factor loadings (FL) were projected on the FoV for each EOF (see Rubio et al. 2020). They were calculated as the correlation between the cover within a grid cell for each EOF and can range from -1 to +1. The resulting map shows the contribution of each grid cell to the different scales of temporal variability, where high coverage (i.e. positive grid cells) correspond to years

with positive coordinates. Negative grid cells correspond to higher coverage to the time scales with negative values.

Finally, Statistics on the migration of mussel individuals were computed. The distance travelled by moving mussel individuals was extracted from their initial and final positions on the substratum. Additionally, average mussel speed was estimated by dividing their travelling distance with the time elapsed between two observations. Cosines and sines were derived from the vector of the distance travelled. As we suspected different patterns of migration between mussels moving from the assemblage to the bare substratum to those staying within the initial assemblage, the two groups were separated for the statistical analysis. A Mann-Whitney U test was applied on the sines and cosines of their trajectories to test for differences in direction (Table 1).

***Segonzacia mesatlantica* spatio-temporal distribution** - Whittaker-Robinson periodograms ($n = 499$) were used to screen for tidal periodicity in infra-daily crab abundance after removal of the linear trend in the data (2012-2015, Table 1). To identify occupancy differences across substrata, infra-daily observations from 2012 to 2015 were subsampled at a 10-day time interval to fit the observation time step of the years 2015 to 2019 (Table 1). A Friedman non-parametric test (Mack and Skillings 1980) was used to compare mean crab densities among substratum types. If significant, a Wilcoxon-Nemenyi-McDonald-Thompson post-hoc test was performed between pairs of substratum types (Hollander and Wolfe 1999). The influence of substratum type on the distribution of this mobile species was evaluated by calculating the average nearest distance of individuals from the different substrata.

Environmental conditions of assemblages/substrata - Physico-chemical data were used to characterise species niches and environmental conditions on the different substrata. Annotations in the FoV were linked with the closest — in space and time — iButton®

recording, using a circular buffer zone of 5 cm in radius. In addition, *in situ* CHEMINI and temperature measurements were assigned to each assemblage and substratum. Distinction was made between ‘densely packed mussels’ and ‘sparsely packed mussels’, because these two assemblages were shown to colonise different habitats (Cuvelier et al. 2009; Husson et al. 2017). ‘Dense’ mussels were defined as large individuals entirely occupying a surface (no bare substratum visible), and ‘sparse’ mussels were more spread out with some substratum visible between individuals (Figure 2A).

Role of temperature on faunal cover - To assess the role of temperature on local changes in mussel and mat cover over time, we computed the spatial distribution of temperatures every month. The data provided by the iButton® probes ($\pm 0.5^\circ\text{C}$) were used to model the dilution gradient from the main vent orifice to different areas in the FoV (5 x 5 cm grid cells). We assumed the size of these cells to be accurate enough to map the dilution gradient of the vent fluid as observed by Podowski et al. (2009). iButton® probes located on the right side of the FoV were discarded due to their lack of visibility. To model the dilution gradient in a dynamic way, least-square linear regressions were performed every month based on the distance of each sensor to the warmest temperature point measured during the whole time series. The mean temperature for each grid cell was extracted (5929 pixels). The lower limit of temperatures in the dilution model was set to 4.7°C (mean temperature on the TEMPO ecological module). EOFs were computed on this new interpolated temperature dataset. To determine the role of changes in temperature on the spatio-temporal distribution of biological components, these EOFs were compared with those of *B. azoricus* and microbial mat cover using the Pearson correlation coefficient (Rubio et al. 2020). All figures and analyses were performed in Python (v. 3.7) and R (v. 3.3.2.; R Core Team 2016). Details on the results of EOF correlations are available in the Supplementary Data.

3. Results

3.1. Scene description and evolution

The FoV was separated into several zones corresponding to the presence of fauna, microbial mats or substratum types (Figure 2). Biological features included a distinct assemblage of *B. azoricus* mussels, zoanthid patches and microbial mats. The mussel assemblage extended more than 1 m upward on a vertical wall above the active hydrothermal diffusion zone. Mussel size varied with increasing distance from the vent orifice, with larger individuals forming a denser patch closer to the vent (Figure 2). The dark substratum was identified as hydrothermal slab of breccia (Pelleter E., pers. comm.). The slab substratum was either bare or covered by white material of unknown nature. One main active source of translucent fluid and secondary small diffusing zones were identified within the FoV (Figure 2). Starting from 2015, the centre of the image featured the growth of a thin spire which repeatedly collapsed and regrew, before eventually being colonised by a few large mussel individuals (Supplementary Figure 3). We also observed the growth of a lateral outcrop in March 2016, resulting in a ~10-cm diameter flange by the end of the 2018-2019 period (Supplementary Figure 4). Finally, no major change in the FoV was observed over the entire study period, except for a slab rock of roughly 1 m that broke into two pieces and slid horizontally towards the mussel assemblage between April 2015 and September 2016 (Supplementary Figure 5).

3.2. Long-term dynamics of the fauna and microbial mats

3.2.1. *Bathymodiolus azoricus*

Occupancy and temporal changes - The area that mussels occupied reached a maximum of 37.4% of the total area in 2012-2015 (large FoV) and 51.8% in 2012-2019 (small FoV). The mussel cover recorded in the large FoV from 2012-2015 was stable, ranging between 19.25 and 22.14 dm² (Figure 3A). The smaller area captured by the full image set from 2012 to 2019 displayed more changes, with cover varying between 5.89 and 11.62 dm² (Figure 3B).

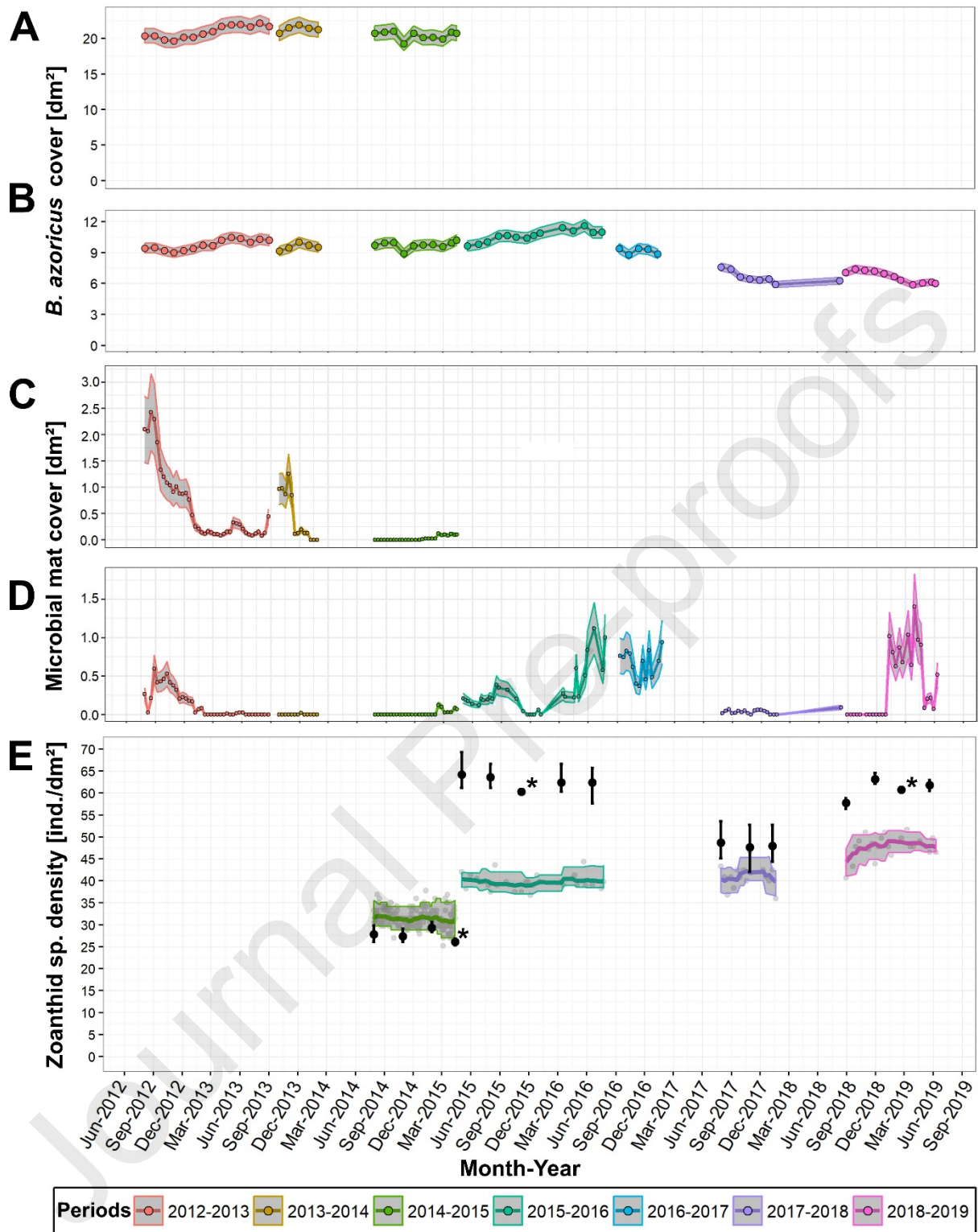


Figure 3 – Total cover annotated for (A-B) the mussel *Bathymodiolus azoricus* (monthly; e.g. Figure 2A), (C-D) microbial mats (7 to 10 days; e.g. Figure 2D) using different fields of view (FoVs): (A & C) the large FoV, recorded from 2012 to 2015 (75.85 dm²), comprising (B & D) the small FoV, recorded from 2012 to 2019 (35.66 dm²; see Figure 2). Colours refer to periods delimited by the deployment and recovery of the TEMPO ecological module at the base of the active Eiffel Tower edifice (Lucky Strike vent field, Mid-Atlantic Ridge). Grey areas depict the intervals of annotation errors estimated for total mussel

cover ($\pm 5\%$) and microbial mat cover ($\pm 30\%$). E. Zoanthid density plotted over time (e.g. Figure 2B). Lines refer to automated density data averaged over a monthly period. Grey areas refer to the associated 5-95th percentiles. Grey circles represent density values extracted from automatic detection. Black circles and bars represent the mean density and range, respectively, for three-replicate manual annotations for validation of the automated detection routine. Asterisks indicate that annotation replicates gave the same density values.

Table 2 – Results of least-square linear regressions applied on periods of mussel total cover recorded in two fields of view (FoVs) (Figure 3A & 3B). Only slope values are given with their associated adjusted R², degrees of freedom (df) and F-statistics. Significant slopes are indicated with asterisks (*p*-value: * < 0.05, ** < 0.01, *** < 0.001). ¹Only 6 months of data from 30 July 2017 to 19 January 2018 and from 29 September 2018 to 30 March 2019.

FoV	Period	Slope [dm ² /month]	Adjusted R ²	df	F-statistic
2012-2015	2012-2013	+ 0.19***	0.74	12	36.85
	2013-2014	+ 0.10	- 0.15	3	0.46
	2014-2015	- 0.03	- 0.11	8	0.14
2012-2019	2012-2013	+ 0.10***	0.66	12	26.20
	2013-2014	+ 0.10	0.00	3	1.01
	2014-2015	+ 0.03	- 0.05	8	0.54
	2015-2016	+ 0.11***	0.72	12	34.58
	2016-2017	- 0.06	-0.21	3	0.30
	2017-2018	- 0.10	0.35	6	4.75
	2018-2019	- 0.16	0.82	9	46.24
	2017-2018 ¹	- 0.27**	0.84	5	31.75
2018-2019 ¹	- 0.26***	0.92	5	73.83	

A significant linear increase in *B. azoricus* cover occurred during the 2012-2013 period in both FoVs (Table 2, Figure 3A & 3B). Variations in 2013-2014 and 2014-2015 were smaller than the annotation error ($\pm 5\%$) and no significant trend was detected (Figure 3B). From 2015 to 2016, the cover significantly increased (Table 2) and started decreasing in September 2016 until the end of the time series. Two periods were particularly noteworthy, with major cover loss: (1) August 2017 to mid-January 2018 with -0.27 dm²/month (Table 2) and (2) October 2018 to April 2019 with -0.26 dm²/month (Table 2).

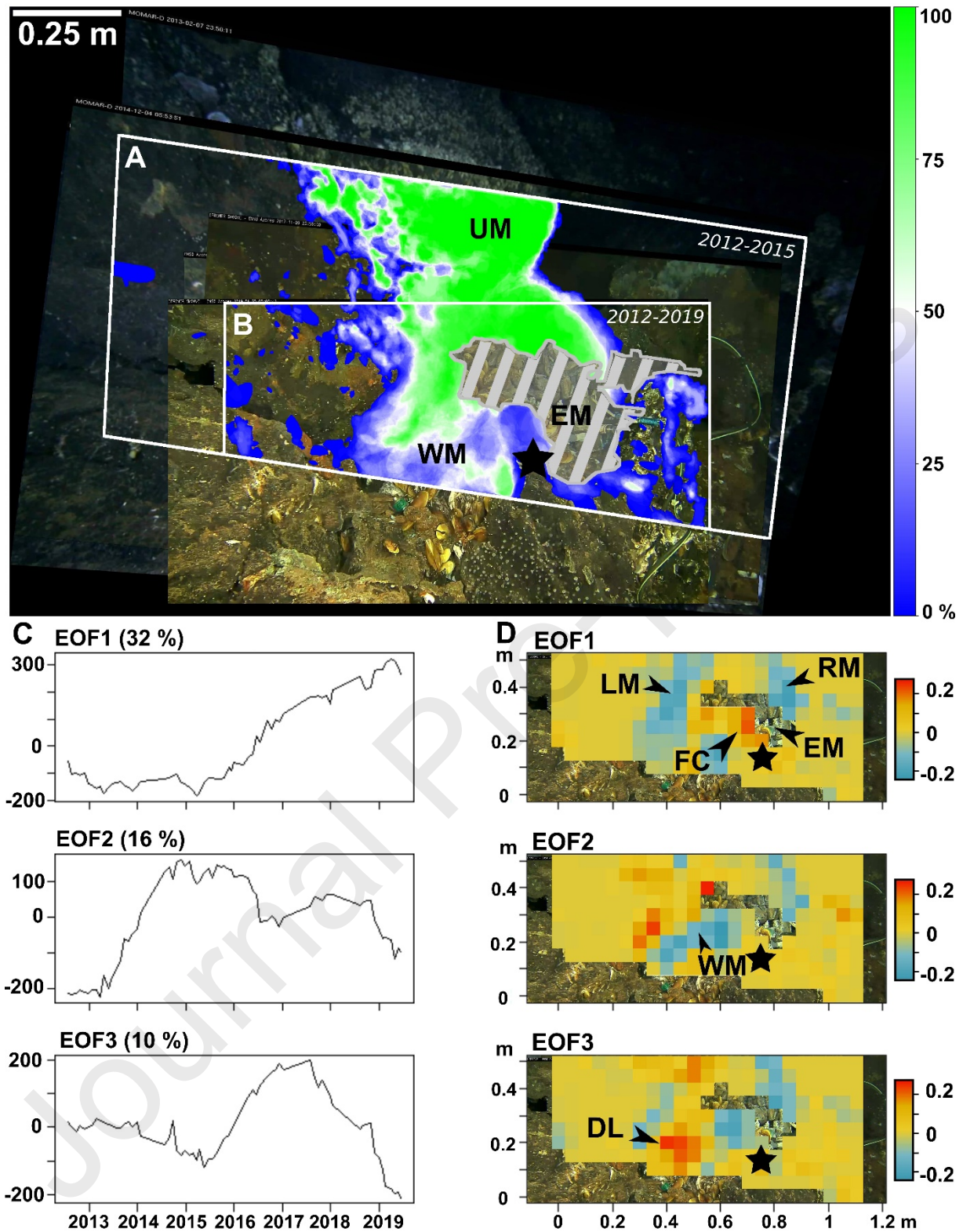


Figure 4 – (A-B) Maps of mean occurrence showing *Bathymodiolus azoricus* mussel cover distribution through time. The area occupied by the environmental module during the whole time series is hatched in grey. The colour gradient refers to the percentage of images displaying mussel cover at a given pixel (0% means full transparency): (A) for the large field of view (FoV) from 2012 to 2015 and (B) for the small FoV from 2012 to 2019. The white scale bar indicates an estimated length of 0.25 m. (C-D) Results of the empirical orthogonal function (EOF) analysis to identify areas with different temporal patterns of

variability. It was undertaken on a time x space matrix where space (i.e. 2012-2015 FoV) is divided in multiple cells of 5 x 5 cm. (C) Time series representing the coordinates of each observation date on the first 3 EOFs (variance explained = 58%). (D) Spatial projection of the factor loadings (FL) of each EOF. The grid cells are coloured according to the degree of correlation between the mussel cover of each grid cell and the given EOF time series. Red cells (positive values in Figure 4D) indicate spatial patterns in years with positive coordinates (Figure 4C), whereas blue cells (negative values) indicate other spatial patterns mainly observable in years with negative values. All metadata related to data acquisition and extraction are presented in Table 1. UM: upper mussel assemblage, EM: Environmental module, WM: white material, LM: left mussel assemblage, RM: right mussel assemblage, FC: flange colonisation, DL: downward loss. Black star: vent orifice.

The small and large FoVs are both occupied by a highly variable zone around the main vent orifice (WM in Figure 4B). The large FoV also contains a portion of the mussel assemblage that is not present in the small FOV (UM in Figure 4A) and that only exhibited minor changes (Figure 3A). Given that EOFs computed for the large 2012-2015 FoV captured the same spatio-temporal structure as the small 2012-2019 FoV (Figure 4D), only the results of the latter are presented because it covers a longer time period (Supplementary Figure 6). The first three EOFs computed for the 2012-2019 FoV accounted for 58% of the total variance in spatial mussel cover (Figure 4C). FLs described a poor correlation between local mussel cover and all three EOFs (FLs ranging from -0.24 to 0.26, Figure 5D). EOF1 explained 32% of the total variance and underlined a progressive change in cover distribution starting from mid-2015 until 2019. As supported by observation in images (Supplementary Video 1), this change corresponded to (i) a 15-cm displacement of the mussel assemblage to the right starting from 2015 (negative FLs, LM in Figure 4D), (ii) the disappearance of patches of small mussels that had settled in October 2013 in 2016-2017 (negative FLs, LM in Figure 4D) and (iii) the colonisation of an area of 2.98 dm² on top of a growing flange by large mussels, from January 2017 to June 2019 (positive FLs, FC in Figure 4D; Supplementary Figure 3). The variability observed at the upper right edge of the mussel assemblage (RM in Figure 4D) and captured by all EOFs corresponds to a loss of mussel cover (negative FLs; Figure 4D). Visual variability of mussel cover in the

white material coincided with EOF2-3 explaining part of the remaining variance (26%). This variability highlights frequent changes in cover distribution in this area (WD in Figures 4B & D). EOF3 identified a decrease in a patch of large mussels initially located on the white material (DL in Figure 4D), which corresponds to a decrease in cover in July 2017 (Figure 3B).

Migration – Thirty-six mussel individuals were observed migrating onto the bare substratum, which represented ~12% of the assemblage population counted in the large FoV (~300 individuals, 2012-2015; see examples in Supplementary Figure 7). Of the 28 individuals that were first observed on the slab substratum, 5 reached the main assemblage. Of the 8 individuals that left the mussel assemblage for the bare substratum, 6 returned to the assemblage. Significant differences in the horizontal direction displacement (i.e. cosines) suggested that mussels isolated on the bare substratum moved preferentially to the right, towards the main assemblage (Mann-Whitney U, $W = 614$, $p = 0.038$; mean cosine \pm SD = 0.39 ± 0.72), compared with the 24 mussels located in the assemblage that favoured vertical movements (mean cosine \pm SD = 0.14 ± 0.63). Mussel tracking showed that 11.25% of the displacements were greater than 10 cm in 6 h with a maximum average speed of 4.66 cm/h.

3.2.2. Microbial mats

Microbial mat cover varied from null to 2.43 dm² in the large 2012-2015 FoV and were present over a continuous period representing 77.5% of the images (Figure 3C). Two main periods characterised by mat cover exceeding 0.5 dm² were identified and both lasted at least 2.5 months. The total microbial mat cover underwent a progressive decrease from September 2012 and stabilised around 0.1 dm² by the end of January 2013 (Figure 3C). A new peak was recorded for 3 months between the end of August and the beginning of November 2013, after which the microbial mat cover declined at an average rate of -0.07 dm²/day. Cover was null by the beginning of January 2014 and the absence of microbial mats lasted until mid-December 2014

(Figure 3C). When considering the small 2012-2019 FoV, total mat cover varied from null to 1.4 dm². During this period, 41.2% of the 170 images analysed did not show any microbial mat cover (Figure 3D). Four episodes of increase (in 2012, 2015, 2016 and 2019) varying in duration and separated by null cover periods were identified with covers ranging from 0.4 dm² to 1.4 dm² (Figure 3D). The most abrupt rates of change reached in average 0.08 dm²/day for two episodes of growth in January and March 2019 and for a decline in April 2019 (Figure 3D). Overall, microbial mats were mainly observed on the left side of the FoV in the vicinity of the mussel assemblage (VM in Figure 5A & B).

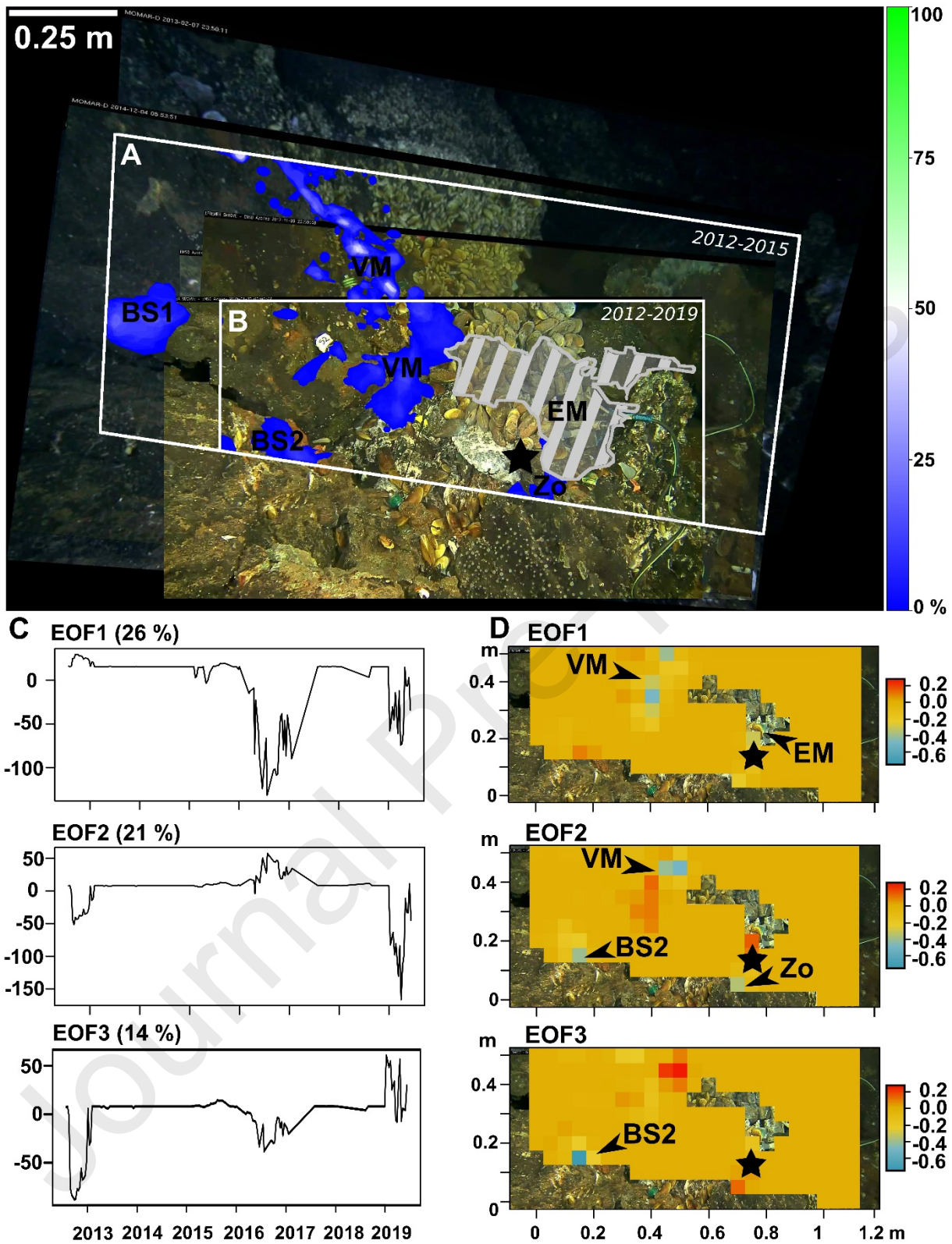


Figure 5 - (A-B) Maps of mean occurrence showing microbial mat cover distribution through time. The area occupied by the environmental module during the whole time series is hatched in grey. The colour gradient refers to the percentage of images displaying microbial mat cover at a given pixel (0% means full transparency): (A) for the large field of view (FoV) from 2012 to 2015 and (B) for the small FoV from 2012 to 2019. The white scale bar indicates an estimated length of 0.25 m. (C-D)

Results of the empirical orthogonal function (EOF) analysis to identify areas with different temporal patterns of variability. It was undertaken on a time x space matrix where space (i.e. 2012-2015 FoV) is divided in multiple cells of 5 x 5 cm. (C) Time series representing the coordinates of each observation date on the first 3 EOFs (variance explained = 61%). (D) Spatial projection of the factor loadings (FL) of each EOF. The grid cells are coloured according to the degree of correlation between the mussel cover of each grid cell and the given EOF time series. Red cells (positive values in Figure 5D) indicate spatial patterns in years with positive coordinates (Figure 5C), whereas blue cells (negative values) indicate other spatial patterns mainly observable in years with negative values. All metadata related to data acquisition and extraction are presented in Table 1. VM: vicinity of the mussel assemblage, EM: environmental module, BS1 & BS2: bare substratum, Zo: zoanthids, Black star: vent orifice.

Two patches also developed >1 m away to the left of the mussel assemblage (BS1 & BS2 in Figure 5A & B) and within the zoanthid assemblage at the bottom of the FoV (Zo in Figure 5A & B). No mat was observed on the right side of the hydrothermal vent orifice (Figure 5A & B). The first three EOFs accounted for 61% of the variance. FLs varied from -0.73 to 0.27, suggesting strong spatial structure in temporal variability. Results showed that changes in spatial patterns of mat cover occurred at a scale of 3 to 6 months (Figure 5C). EOF1 explained 26% of the total variance and corresponded to the repeated development and decline of microbial mats in the vicinity of the mussel assemblage in 2016 and 2019 (FL < -0.4; VM in Figure 5C & D). EOF2 accounted for 21% of the variance and corresponded to mats occurring at the same time in three distinct areas in 2012 and 2019 (FLs < -0.3): in the vicinity of the mussel assemblage (VM), on bare substratum on the left of the FoV (BS2), and within the zoanthid assemblage (Zo in Figure 5D). EOF3 (14% of the variance) revealed the dynamics of a single patch located on the bare substratum that developed in 2012 and in 2016 (FL < -0.6; BS2 in Figure 5D). EOF results for mat redundancy in the large 2012-2015 FoV highlight additional variations on the slab located on the left side of the FoV (BS1 in Figure 5A; EOFs in Supplementary Figure 8), away from mussel patches. The dynamics of these patches, i.e. lifetime of a patch, were similar to those in the small FoV, i.e. from 2 to 7 months

(Supplementary Figure 8). Dynamics observed in images are provided in Supplementary Video 2.

3.2.3. Zoanthids

Manual annotations of zoanthids resulted in a minimum of 25.4 ind.dm⁻² and a maximum of 69.3 ind.dm⁻² compared with a minimum of 25.2 ind.dm⁻² and a maximum of 51.7 ind.dm⁻² for the automated algorithm (Figure 3E; Supplementary Figure 9). The manual and automated detection methods differed in terms of absolute density, but depicted the same pattern over time (Figure 3E). The dispersion of the points differed among periods, with a maximum of 22.5% in November 2017 based on manual annotations.

3.2.4. *Segonzacia mesatlantica*

A total of 2600 crabs were counted from 2012 to 2019. The abundance of crabs reached a maximum of 7 individuals in one image, and 26.2% of the 3120 images revealed no individuals. Significant tidal periodicity was not detected in crab abundances. Infra-daily observations from 2012 to 2015 were subsampled at a 10-day time interval. The large 2012-2015 (n = 80 crabs) and small 2012-2019 (n = 326 crabs) FoVs were both analysed, but because 90% of the crabs present in the large FoV were already included in the small FoV, only results from the latter are presented (Supplementary Figure 10A- B). 50.9% of the 326 crabs were detected on the mussel assemblage, 27.9% on the white material, 18.4% on the bare substratum, 2.5% on the environmental module, 0.3% in crevices, and none on microbial mats (Supplementary Figure 11). Crab observations for both time series displayed significant differences in densities among substratum types (2012-2019; Friedman chi-squared = 279.53, df = 5, $p < 2.2e-16$). Post hoc tests revealed significantly higher occupancy in the mussel assemblage (Mean density \pm SD = 0.14 ± 0.13 ind./dm²) and on the hydrothermal white material (0.15 ± 0.13 ind./dm²) than on microbial mats (0 ind./dm²), crevices (0.01 ± 0.1 ind./dm²), slab substratum (0.01 ± 0.02

ind./dm²) and the environmental module (0.02 ± 0.1 ind./dm²). Furthermore, we noticed that crabs, when located on the slab substratum, occupied areas close to the mussel assemblage (mean distance \pm SD = 1.8 ± 2 cm, maximum distance of 8.6 cm, Supplementary Figure 11A).

3.3. Biotic interactions

Avoidance behaviour of smaller mussel individuals were occasionally observed after the arrival of larger mussels in close vicinity (e.g. Supplementary Figure 12A). Small mussels carried by larger ones were sighted in zoomed-in video sequences (e.g. Supplementary Figure 12B). Over the whole set of video sequences, no feeding behaviour of crabs or fish were observed. Crabs occasionally attempted to open mussels or to catch approaching individuals of *M. fortunata* without success. Fish such as *Cataetyx laticeps* Koefoed, 1927 were observed swimming to stay in the FoV and *Gaidropsarus mauli* Biscoito & Saldanha, 2018 were often found on the bottom within crevices. *Synphobranchus kaupii* Johnson, 1862 were occasionally observed visiting the crevices and the assemblages.

3.4. Environmental characterisation

3.4.1. Temporal variability of environmental conditions

Overall, dissolved iron concentrations ranged from 0.1 μ mol/L in July 2017 to 49.5 μ mol/L in November 2018 (Figure 6A). Time series were characterised by discrete changes ranging from 0 to 10 μ mol/L. The average temperatures were $6.8 \pm 6^\circ\text{C}$ and $9.6 \pm 9.4^\circ\text{C}$ as measured by the CHEMINI sampler and the optode probes, respectively. Values ranged from 4.4°C to 114°C (CHEMINI sampler) and 148°C (optode), these latter values being exceptional occurrences and probably most likely related to probe positioning (Figure 6B & 6D). Temperatures exhibited a sharp increase during the 2018-2019 period when the highest value was measured (Figure 6B & 6D). Overall, dissolved oxygen concentrations ranged from 0 to 327.7 μ mol/L with an average of 172.1 ± 92.6 μ mol/L. The 2012-2013 period showed a progressive decline in oxygen

concentrations, but the 2014-2015 displayed a progressive increase, stabilising between 150 and 200 $\mu\text{mol/L}$ (Figure 6C). Oxygen concentrations displayed sharp monthly variability, except in 2016-2017 when they were more stable. Image observation suggested that the position of the TEMPO environmental module can change slightly during the time series. Hydrothermal deposits formed on the module during the 2018-2019 period (authors' pers. obs.).

The turbidity time series, measured at SeaMON East, 10 m from TEMPO, displayed occasional peaks and progressive increases starting around March-June (Figure 6E). Bottom seawater temperature was stable throughout the entire time series (mean \pm SD = $4.7 \pm 0.1^\circ\text{C}$, Figure 6F), exceeding 5°C in less than 1% of the measurements.

No significant periodicity was observed for iron concentrations, as shown by the Whittaker-Robinson periodogram outcomes (Figure 6A). Most temperature time series displayed significant semi-diurnal and diurnal tidal periodicities (Figure 6B, 6D & 6F). Significant tidal periodicities were observed in dissolved oxygen concentrations in 2016-2017 (Figure 6C). No significant tidal periodicity was observed in turbidity (Figure 6E). For the 7-day temperature time series measured every month by the iButton® sensors, 31.8% exhibited significant periodicities at periods of $12.5 \text{ h} \pm 1 \text{ h}$ and 38.5% at periods of $25 \text{ h} \pm 1 \text{ h}$.

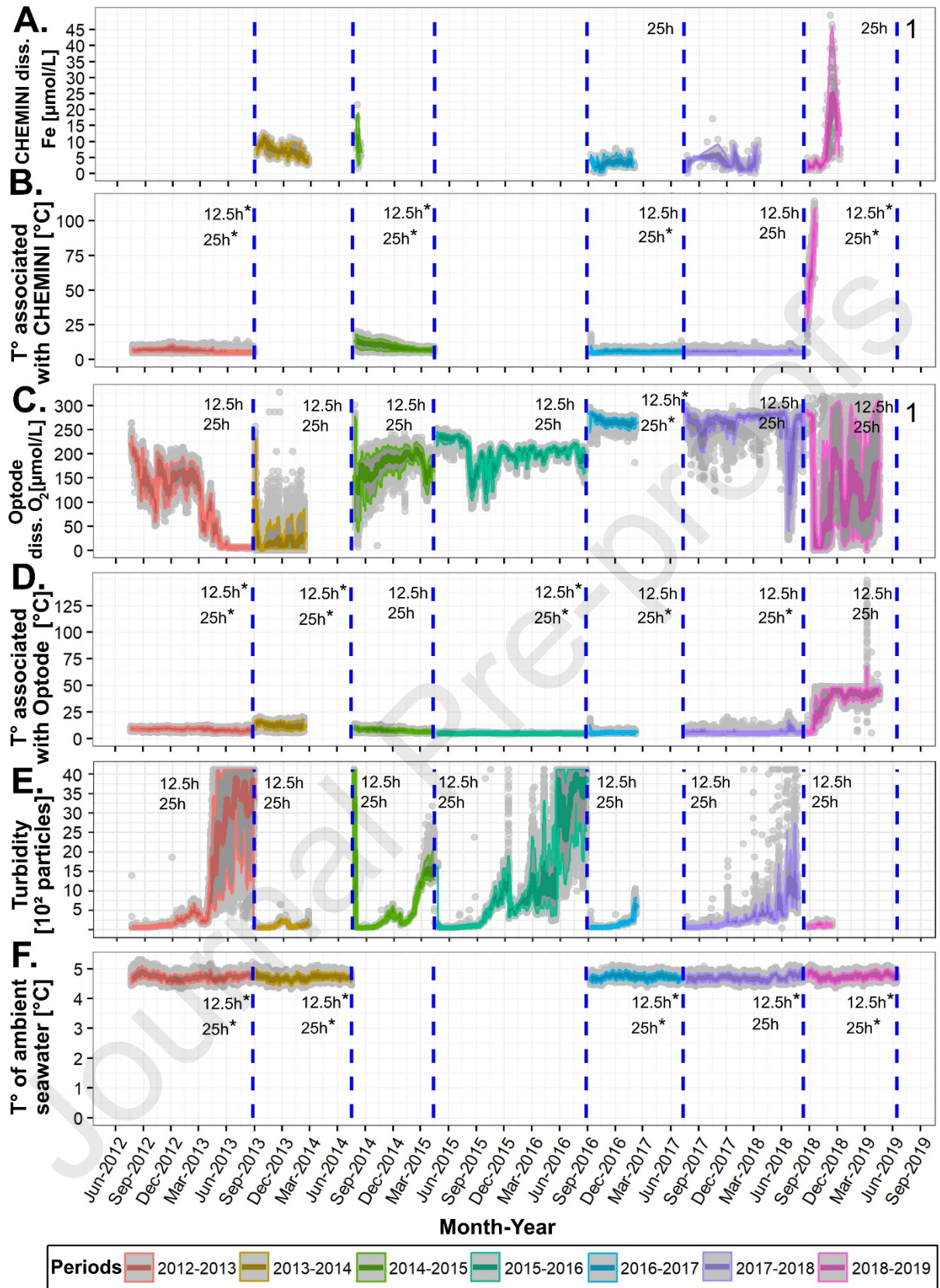


Figure 6 – (A-B-C-D) Environmental data recorded within the field of view (FoV) monitored by the TEMPO environmental module deployed at the base of the active Eiffel Tower edifice (Lucky Strike vent field, Mid-Atlantic Ridge). (A) Dissolved iron [Fe(II) + Fe(III)] concentrations [$\mu\text{mol/L}$] measured by a CHEMINI *in situ* analyser. (B) Temperature [$^{\circ}\text{C}$] measured by

a high-temperature probe positioned next to CHEMINI. (C) Dissolved oxygen concentrations [$\mu\text{mol/L}$] measured by an Aanderaa optode probe. (D) Temperature [$^{\circ}\text{C}$] measured by the probe associated with the optode. (E-F) Background environmental data measured outside the FoV. (E) Turbidity [10^2 particles counted] measured on the SeaMON East node 10 metres away from the TEMPO ecological module. (F) Temperature [$^{\circ}\text{C}$] on the TEMPO ecological module. Grey areas depict the associated 5-95th percentiles. Grey circles represent values measured with the sensors. Dashed blue lines delimit periods of data acquisition, defined by the deployment and recovery of the sensors during the yearly MoMARSAT cruises. 12.5 h and 25 h indicate if a Whittaker-Robinson periodogram was generated to test for tidal periodicity. * indicates significant periodicity ($p < 0.05$). (1) Note: the temperature associated with CHEMINI and optode probes reached over 100°C ; therefore, the environmental module may have been dysfunctional for the 2018-2019 period.

3.4.2. Spatial variability of environmental conditions

Monthly temperatures measured by iButton® probes and averaged over one week showed that *B. azoricus* and microbial mats occupied areas in which mean temperatures were 6.8°C and 5.8°C , respectively, while crabs were observed in warmer habitats with a mean of 9.8°C (Table 3). Moreover, *B. azoricus* and *S. mesatlantica* were present in more variable habitats in which temperatures can exceed 20°C (see maximum temperature, Table 3). Larger mussels were found in warmer and more variable temperatures (Mean \pm SD = $6.2 \pm 1.5^{\circ}\text{C}$) than smaller mussels ($5.0 \pm 0.1^{\circ}\text{C}$). The sparse mussel assemblages occupied colder microhabitats less exposed to the hydrothermal outflow with lower concentrations of dissolved iron and total sulphide (Table 3, Supplementary Figure 13). Average temperature was 9.5°C with a maximum of 25.1°C on the white material (Table 3), where white substratum accretion dynamics was observed (Figure 7A). Temperatures measured away from that point were stable over the years, with the exception of a few points recorded in a small area 20-30 cm away that briefly exceeded 10.0°C in 2018-2019 (Figure 7A; Supplementary Figure 14).

Measurements with the submersible probes during yearly cruises led to similar results. The maximum temperature measured in the vent orifice with these probes reached 133.8°C , and all

Table 3 – Environmental factors measured in the TEMPO ecological observation module (EMSO-Azores observatory) field of view: (A) Yearly submersible measurements (n = 116) of temperature for 1 minute (n = 87) and CHEMINI analysers (dissolved Fe(II) [n = 77] and total sulphide concentrations [n = 99]) from 2014 to 2019. (B) iButton® probe temperatures repositioned monthly by annotating their position in TEMPO images from 2014 to 2019. Average temperatures using continuous recordings were retrieved automatically using a temporal window of 1 week (± 0.5 °C) (n = 21,988). The maximum weekly average temperature is also given. Measurements were assigned to substratum and taxa based on the visual position of the submersible probes during dives (A) or considering a buffer zone with a radius of 5 cm around the iButton® probes (B). When iButton® temperature sensors were not linked to any particular substratum/taxon, temperature was assigned to the “no cover” class, i.e. the slab substratum. Classes (i.e. columns) are arranged according to the empirical distance of biological features (assemblage type or dominant taxon) and substrata to the vent orifice commonly observed at the hydrothermal edifice Eiffel Tower (Lucky Strike vent field; Cuvelier et al., 2009; Girard et al., 2020). Arrows indicate this theoretical gradient of the fluid dilution. No standard deviation refers to single point measurements.

Environmental factor		←	←	←	←	Hydrothermal vent orifice	→	Farthest from the vent orifice	
		Zoanthids	Microbial mat	Biological features		Close vicinity to the vent orifice	White material	Slab substratum	
				Sparse <i>Bathymodiolus azoricus</i> assemblage	Dense <i>Bathymodiolus azoricus</i> assemblage	<i>Segonzacia mesatlantica</i>			
(A) Data collected during submersible dives	Mean temperature \pm SD [°C]	5.1	<i>No data</i>	5.0 \pm 0.1	6.2 \pm 1.5	<i>No data</i>	39.1 \pm 36.4	5.8 \pm 0.4	4.9 \pm 0.4
	Mean Fe concentration \pm SD [μ mol/L]	0.4	1.6	1.2 \pm 2.9	1.1 \pm 1.2	<i>No data</i>	9.0 \pm 14.2	0.3 \pm 0.5	1.3 \pm 2.2
	Mean sulphur concentration \pm SD [μ mol/L]	7.4 \pm 9.0	15.4	5.0 \pm 7.9	19.0 \pm 28.0	<i>No data</i>	107.2 \pm 105.8	12.0 \pm 13.9	10.9 \pm 25.7
(B) Data collected via iButton® probes	Mean temperature \pm SD [°C]	<i>No data</i>	5.8 \pm 0.2	<i>(no distinction made in cover type)</i> 6.8 \pm 3.2		9.8 \pm 6.0	<i>No data</i>	9.5 \pm 5.2	6.2 \pm 1.6
	Maximum temperature [°C]	<i>No data</i>	6.0	25.1	23.8	<i>No data</i>	25.1	12.7	

measurements in the surrounding microhabitats were below 10°C illustrating sharp, centimetre-scale spatial variability (Supplementary Figure 13). Total sulphide concentrations and temperature were good indicators of fluid dilution and were used to discriminate habitats within the FoV according to a theoretical zonation of hydrothermal fluids along the mixing gradient (Table 3). Standard deviations of the measured physico-chemical factors were on average higher and more variable closer to the vent orifice. Dissolved iron concentrations were higher in microbial mats and in sparse mussel patches than in dense mussel assemblage. The bare substratum was characterised by higher iron concentrations than the white material (Table 3).

3.4.3. Environmental drivers of change

EOF analyses applied on gridded temperatures revealed two major temporal patterns that explained 99% of the total variance. FL values suggested a poor correlation between temperature and EOFs ($FL < |0.2|$, Figure 7C). EOF1 was related to larger variations closest to the vent orifice, accounting for 85% of the variance with increased temperatures in 2015, 2018 and 2019 ($FL \sim 0.2$; Figure 7B & C). EOF2 accounted for 14% of the variance and captured the opposite relationship between the warmest areas, strongly influenced by the hydrothermal outflow and an area on the left side of the FoV where temperatures fluctuate depending on the dilution gradient ($FL \sim 0.15$; Figure 7C). The top left grid cell remained poorly affected by fluctuation of the hydrothermal fluid temperature (Figure 7B & C).

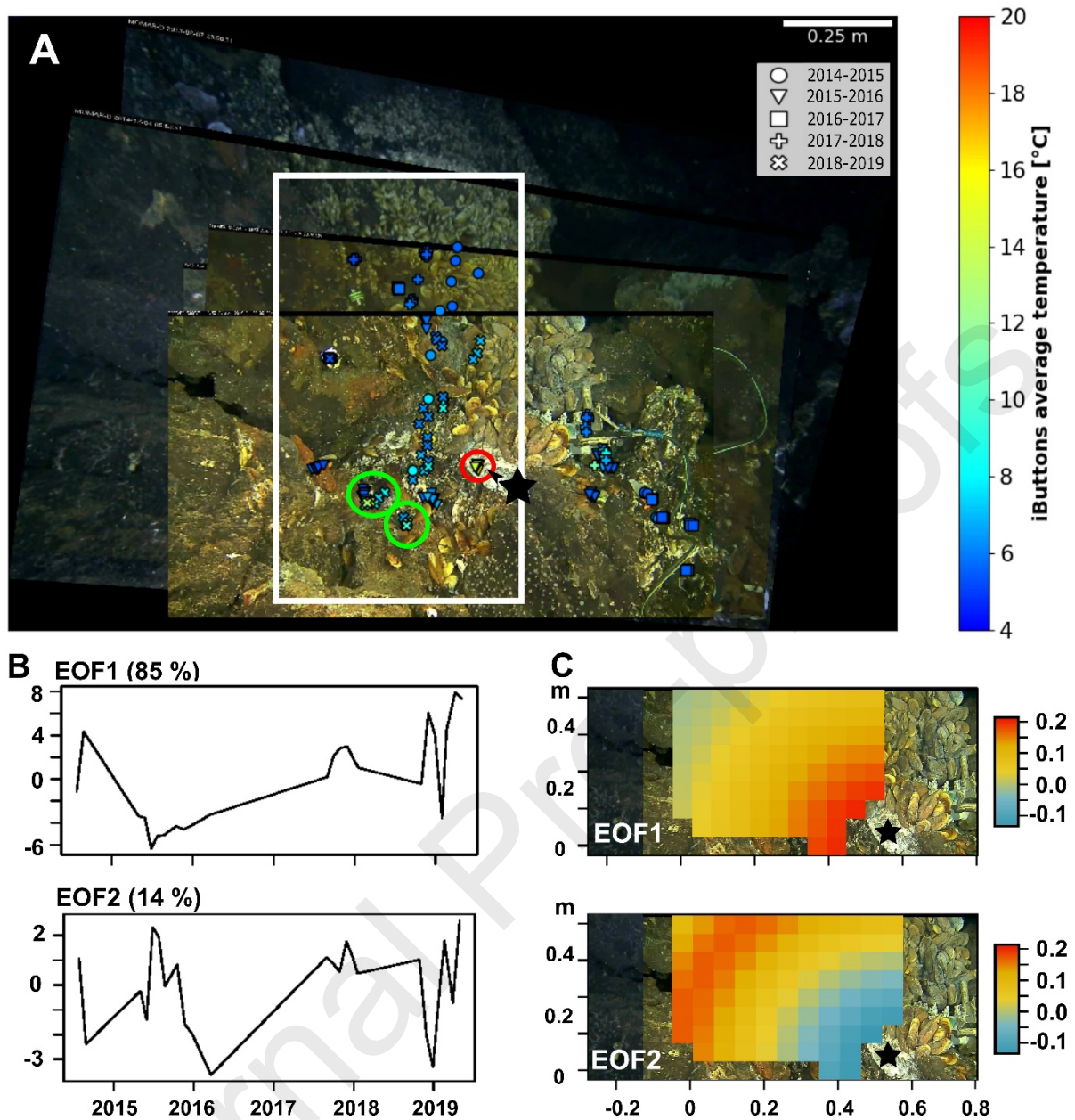


Figure 7 - Spatio-temporal analysis of the temperature recorded by the iButton® sensors averaged over a weekly interval every month. Black stars: vent orifice. (A) Spatial distribution of the measurements. Colour bar refers to temperature values [°C]. Red circle: the warmest temperatures recorded by temperature sensors. Linear regressions were based on the distance from that location using monthly temperatures. White box: only iButtons® from this side of the vent orifice were used to perform linear regressions. Green circle: locations of temperature anomalies (+2 to 5 °C). (B-C) Results of the Empirical Orthogonal Function (EOF) analysis undertaken on a time x space matrix where space (i.e. 2012-2019 FoV) is divided in multiple cells of 5 x 5 cm. (B) Time series of the first two EOFs representing the coordinates of each observation date along the first two EOFs (variance explained = 99%). (C) Spatial projection of the factor loadings (FL) of each EOF. The grid cells are coloured according to the degree of correlation between the local temperature time series of each grid cell and the given EOF time series (Figure 7B). All metadata related to data acquisition and extraction are presented in Table 1.

EOFs of gridded temperatures were poorly correlated with those of microbial mats ($p < 0.05$). Only temperature EOF1 and microbial mat EOF2 displayed a negative relationship (Pearson $r = -0.46$, $t = -2.3629$, $p = 0.028$) and corresponded to changes that occurred in 2012 and 2019. *B. azoricus* EOF1 was correlated with temperature EOF1 (Pearson $r = 0.64$, $t = 3.3131$, $p = 0.0044$) and EOF2 (Pearson $r = -0.64$, $t = -3.2992$, $p = 0.0045$). These correlations suggest a stronger link with temperature dynamics in the warmest areas. Finally, the three first EOFs of microbial mats showed significant correlations with those of *B. azoricus* for 7 EOF pairs out of 16 (Pearson r , $p < 0.05$, see details in Supplementary Data). A closer look with zoomed-in videos showed that the appearance of microbial mats interlaced within the byssus threads (VM in Figure 5D) coincided with the departure of mussels (LM in Figure 4D).

4. Discussion

The EMSO-Azores observatory provides an unprecedented time series of biological and associated environmental data for a vent ecosystem. Imagery is non-destructive method, making it an ideal approach for the long-term study of vent communities (Tunnicliffe 1990; Sarrazin and Juniper 1998). The data analysed in this study constitutes the longest imagery time series of a vent faunal assemblage with high temporal resolution and is the first compilation of observatory-sourced biological data over a 7-year acquisition period. This novel approach, coupling spatial and temporal analyses, provides a baseline workflow, highly valuable for future observatory studies.

4.1. Limitations

Our study highlighted two main limitations that need to be kept in mind when interpreting the results. First, this study assessed a limited range of spatial scales. Although we can examine the underlying mechanisms of processes shaping ecological dynamics at the assemblage scale, our results cannot simply be extrapolated to larger scales (Levin 1992; Underwood et al. 2005;

Gonzalez et al. 2020). Indeed, ecological processes are expected to change with increases in the spatial, temporal and organisational scales of the study from individuals to meta-communities, because larger scales may encompass a greater range of environmental conditions and biological features (Rosenberg and Freedman 1994; Zajac et al. 1998; Underwood et al. 2005). Seafloor observatory imagery data only provide information on the processes influencing faunal assemblages locally. However, they include a high-resolution time series of concomitant environmental fluctuations at the field scale (e.g. seismic activity, current variations, temperature) that could have impact at local scales. Therefore it is important to couple our observations with surveys at broader scales, also to incorporate a larger range of faunal assemblages and habitat heterogeneity. Nevertheless, despite the limited scale of our study (<1 m²), our yearly presence at the study site (ET) made it possible to gain an integrated understanding of temporal variability at larger scales. At the other end of the spatial range, our image resolution also prevented the evaluation of the role of small-sized fauna (< 1 cm) in assemblage dynamics. The second major limitation involves the position of the recording modules and sensors. Consistency in spatial and temporal observations (i.e. FoV, sampling frequency) and temporal coverage of recordings are required to characterise the long-term evolution of faunal distribution, identify drivers of change and unveil the underlying mechanisms. Unfortunately, the yearly recovery of the TEMPO ecological observation module affected the position of the camera and sensors of the environmental module, which in turn affected the spatial overlap of images and *in situ* measurements along the time series. To solve part of this problem, the use of homography proved to be an efficient tool to retrieve a series of overlapping images, needed for quantitative temporal analyses. However, homography required discarding data from some non-overlapping portions of the image. Further development of the ecological observation module (e.g. pan-and-tilt module) should help optimise the overlapping surface area, as well as the zone under observation to ensure high zoom detail. The long-term

detection of changes in fluid emissions at the assemblage scale was also difficult due to inadvertent small changes in the location of the chemical analyser between years. The surface being monitored undergoes a sharp dilution gradient of vent fluids, meaning that even a small centimetre-scale displacement of the sampler inlet can result in significant physico-chemical changes. In addition, the occasional failure of the optode and CHEMINI analyser (e.g. after accumulation of white material on the inlet) added an element of uncertainty in the time series that could be solved in the future by taking more sampling replicates. Finally, mussel displacement also led to the constant reconfiguration of the iButtons® temperature grid. The use of a solid frame may be necessary to maintain the sensors in the same location.

4.2. Habitat and environmental dynamics

Different types of substrata and geological features were identified in our images. They include a bare substratum identified as the “slab”. This mineral is common at LS and is composed of a hyaloclastite aggregation of basaltic glass, plagioclase crystals and sulphide grains hydrothermally cemented by amorphous silica and baryte (Langmuir et al. 1997; Humphris et al. 2002). A white material was also identified close to the fluid emission. The nature of this material (Figure 2C) was difficult to assess from imagery only (Supplementary Video 3). According to the literature and expert knowledge, it either corresponds to baryte or anhydrite deposits, forming at temperature higher than 60°C for the former (Jamieson et al. 2016) and higher than 150°C for the later (Tivey 2007), or to thin microbial mats such as those produced by *Arcobacter* spp. (Taylor et al. 1999). Temperatures around the vent orifice reached 133.8°C in our study area.

Our time series confirmed the long-term stability of the diffuse flow habitat monitored by TEMPO (H1). On bare substratum, only minor changes were observed. They include the migration of a small group of large mussels aggregated around a patch of white material

between July 2014 and June 2015. The departure of the mussels by the end of November 2015 coincided with the disappearance of the patch (Supplementary Figure 15). Small variations in temperature ($> 4^{\circ}\text{C}$) were also detected on the bare substratum in 2019. Aperiodic variability in temperature measurements could be due to a number of factors, including the relocation of small fluid orifices (Chevaldonné et al. 1991), the deviation of fluids by mussels (Johnson et al. 1994) or to the clogging of vent orifices as observed by (Sarrazin et al. 1997). Our observations showed that temperature changes could also arise from local physical rearrangements, such as the displacement of boulders or the formation of geological features that may contribute to diverting the flow of hydrothermal fluids. Several factors can trigger local changes in temperatures, making it difficult to determine possible causes. The diversity of spatial and temporal scales at which these changes can occur benefits from the use of multidisciplinary observatories that provide an integrated network of physical, chemical, geological and biological data over a wide range of scales that inform on processes occurring at larger scales (e.g. seismic events or change in hydrothermal circulation). Finally, the significant tidal signal detected in temperatures measured over the bare substratum accounted for most of the environmental variability observed in the FoV throughout the time series. The role of tidal external forcing periodically modulating local environmental conditions along vent fluid orifices has often been reported (Chevaldonné et al. 1991; Johnson et al. 1994; Sarrazin et al. 2006, 2014; Cuvelier et al. 2014; Lee et al. 2015; Lelièvre et al. 2017). Semi-diurnal and diurnal tides can modify exposure to fluids through changes in near-inertial bottom currents (Scheirer et al. 2006; Barreyre et al. 2014). Tides also temporarily modify the characteristics of vent emissions (e.g. velocity, seafloor mixing) through variations in seafloor permeability and associated subsurface pressure gradients (Davis and Becker 1999; Pruis and Johnson 2004; Crone and Wilcock 2005).

Moreover, the most prominent changes to the physical habitat were restricted to the friable white material in the central diffuse-flow area. These changes include the formation of two small hydrothermal geological features, i.e. a 10-cm long spire and a 10-cm diameter flange. The growth of the small chimney corresponded with a temperature shift dropping from 30°C (April 2015) to 13°C (March 2016) that was recorded by one of our iButtons® located in the centre of the FoV. The formation of the flange coincided with a likely rearrangement of the plumbing vent system at the field scale in September 2015 as reported by Ballu et al. (2019). This event might have induced changes in physico-chemical conditions and explain the formation of this new feature. Moreover, the TEMPO environmental module, measured large variations in oxygen concentrations and monthly increases in dissolved iron concentrations in certain years, depending on the probe position near the vent orifice. As changes remained near the main outflow (~10-20 cm from the vent orifice), we conclude that there was no major relocation of the vent fluid orifice on a decadal scale within our FoV.

Outside the FoV, temperature data (probe located on the frame of the camera) also recorded the influence of tidal variations on bottom temperatures. Moreover, sporadic increases in turbidity measured 10 m away from the assemblage could result from periodic increases in plume exposure. Indeed, a recent study using the same data showed that tidal-modulated turbidity peaks can coincide with current reversion, causing currents to transport material away from the edifice (Lantéri et al. 2022). The observed increase of turbidity plateauing in June may also be due to an inflow of surface particles on the seafloor, originating from a phytoplankton bloom known to occur in April-June (Khripounoff et al. 2008). Visual observations of increased marine snow at depths of 1700 m in early June at LS tend to support this hypothesis (authors' pers. obs.). However, because the sensor drifted considerably over time, we were not able to explore potential relationships further.

4.3. Dynamics in faunal distribution in relation to abiotic factors

The stability of the *B. azoricus* assemblage was characterised by the presence of a permanent cover with minor local variability, suggesting the apparent steady state of the population and confirming the hypothesis of little change over the long term (H2). This observed stability supports the observations made over a period of 2 years in the same area (Sarrazin et al. 2014) and 14 years at the scale of the entire edifice (ET, Cuvelier et al. 2011b). Our results however provide additional insights in our understanding of the functioning of ET (Cuvelier et al. 2011b). The apparently low mortality rate throughout 7 years indicates low population turnover, which offers additional support for the hypothesis that the ET habitat may have reached its carrying capacity before the start of this study (Cuvelier et al. 2011b). Similarly, mussel growth and recruitment led to only minor changes in mussel cover and had little impact on assemblage dynamics.

As shown for the environmental data, minor faunal changes were restricted to the assemblages located near the vent orifice. The most prominent decimetre-scale redistribution event corresponded to the overall displacement of a mussel assemblage from 2017-2019 and corresponding in time and space with the development of an active flange. In fact, the top of this hydrothermal feature was gradually colonised by large mussels, suggesting that mineralisation and induration may have possibly occurred throughout the directional accretion of the flange. A study at the Endeavour segment of Juan de Fuca Ridge (Sarrazin et al. 2002) proposed that, as the substratum matures (i.e. decrease in porosity), the habitat is less exposed to direct hydrothermal fluid exposure allowing ecological succession to proceed. Substratum maturation may also contribute to a decrease in its instability and friability, making surfaces more suitable for colonisation. In fact, large mussels appeared to have relocated in response to the opening of a new suitable habitat. Mussel migration is potentially the result of a trade-off between physiological tolerance to physico-chemical conditions and nutritional requirements

(De Busserolles et al. 2009; Cuvelier et al. 2011b; also observed in Supplementary Figure 15). Mussel habitat characteristics were in the range of those found previously in terms of temperature and sulphide concentrations (Cuvelier et al. 2011a; Sarrazin et al. 2015; Husson et al. 2017). Large mussels colonised these areas of higher temperature, sulphide and iron concentrations and lower oxygen levels, but also of higher environmental variability. Our study also highlighted the large range of oxygen and iron concentrations that can be tidally modulated. Indeed *B. azoricus* has developed highly-responsive metabolic adaptations to cope with rapid fluctuations of environmental conditions inducing oxidative stress (Company et al. 2006; Demina and Galkin 2008; Bougerol et al. 2015), hypoxia and high-temperature exposure (Boutet et al. 2009). Despite *B. azoricus* robustness, alternating oxic/sulphidic conditions may be required for the adequate growth of vent mussels (Nedoncelle et al. 2015).

The displacement of individual mussels did not significantly affect the dynamics of the assemblage. Fleeting displacements over short distances have already been observed (Childress 1988; Johnson et al. 1994; Govenar et al. 2004), but their influence on distribution dynamics has never been assessed. Our results show that these ‘mobile’ mussels are capable of faster migration than those that are aggregated and bound by their byssus. The migration of these single individuals may be related to the search for suitable habitat due to competition for space or resources. Nevertheless, it remains unclear at what distance and on which time scales *B. azoricus* mussels are able to detect and travel to newly available or more suitable habitats. Directional patterns of displacement indicate the ability of individuals to orientate their migration towards vent orifices to reach optimal conditions, as hypothesised by other authors (Comtet and Desbruyeres 1998; Colaço et al. 2006; Cuvelier et al. 2009; Sen et al. 2014).

Microbial mats occurred in habitats characterised by temperatures ranging from 4.7°C (background seawater) to a maximum of 10°C. Their growth in the vicinity of the zoanthid or mussel assemblages, and on the bare slab away from vent orifice suggests that they develop in

conditions of low hydrothermal inputs as observed in other studies (Cuvelier et al. 2009, 2011a; Husson et al. 2017). Recurrent periods of appearance and disappearance of these mats over weeks to months were interrupted by periods of total absence, thus refuting the hypothesis of long-term stability (H3). This pattern was poorly correlated with measured temperature changes according to EOF analyses: the presence of infra-annual mat dynamics over a period of 7 years contrasts with the pluriannual stability of hydrothermal conditions in the FoV. Therefore, other factors may play a role, including non-measured environmental variables or biotic interactions (see Section 4.4. on biotic interactions).

Zoanthid densities were roughly 25-70 ind./dm², which is within the range of those previously found in samples collected on ET (up to 30 ind./dm²; Sarrazin et al. 2015). Zoanthid density showed little variation over several months, confirming the hypothesis of the high stability of these assemblages (H4). Overall, the distribution of these cnidarians remains poorly characterised at the LS vent field. At ET, they cover large portions of the edifice in areas away from vent orifices and in areas little exposed to currents carrying hydrothermal material (Girard et al. 2020). However, their close association with chemosynthetic bacteria cannot be excluded without further investigation. For example, intracellular associations with sulphur-oxidising bacteria in hexacorallian species have been reported at hydrothermal vents (Goffredi et al. 2021), but have not been studied for the species at ET. The enhanced growth of non-vent sessile fauna in the vicinity of active vents has been reported in previous studies, suggesting that they benefit from allochthonous and chemosynthesis-derived food sources (Erickson et al. 2009, Sarrazin et al. 2006) or from the presence of prey such as copepods (Limén et al. 2008; De Busserolles et al. 2009). Understanding the link between peripheral zoanthid assemblages and hydrothermal activity warrants further investigation into their ecology. Overall, our results confirm the links between the spatio-temporal distribution of vent assemblages and local environmental conditions, including substratum properties (H5).

4.4. Role of biotic interactions

The role of biotic interactions in shaping the dynamics of the assemblages over time could be inferred from daily recording observations over 7 years. Surprisingly, mussel mortality (i.e. observation of empty shells) was rarely observed within the time period and no mass mortality event was recorded, suggesting a life expectancy of at least a decade for *B. azoricus* mussels of this assemblage. Previous studies showed only occasional predation by the crab *S. mesatlantica* as deduced from the presence of damaged mussels (Matabos et al. 2015) and from stomach content analyses (Colaço et al. 2002). These results are in accordance with stable isotope studies that indicate that *S. mesatlantica* crabs are more likely to be scavengers (De Busserolles et al. 2009; Portail et al. 2018). Predation by *Branchipolynoe seepensis* polynoids, found inside 70% of the mussels sampled at LS (Britayev et al. 2007; João et al. 2018), may be a potential stress factor for mussels, but there were only a few unidentified polynoids preying on mussel mantles in zoomed-in videos (Supplementary Video 4). This low evidence for predation supports previous assumptions that, although partial predation exists on endosymbiotic species, it does not result in their death (Urcuyo et al. 2003; review in Govenar 2012). Finally, visiting fishes with different types of activity regimes were occasionally sighted, but no clear interaction with resident vent species was observed.

The reduced occurrence of interacting behaviours and feeding activity suggest that predation may globally play a negligible role in shaping *B. azoricus* assemblages as suggested by other high-resolution studies at ET (Matabos et al. 2015). However, we cannot discount the role played by selective predation on mussel juveniles and recruits. In fact, a recent recolonisation study at a nearby edifice showed that the exclusion of predators leads to an increase in recruitment in mussel assemblages (Marticorena et al. 2021). In that study, crabs preferentially occupied the white material near the vent orifice and mussel assemblages. They may feed on

recruits and juveniles that develop on mussel shells, on small mobile gastropods such as *Peltoospira smaragdina* (authors' pers. obs.) and on microorganisms that potentially constitute the white patches. Microbial mats have indeed been suggested to be a potential food source for *S. mesatlantica* (Portail et al. 2018). These mats may also significantly contribute to the diet of several bacterivorous species, such as small mobile gastropods not visible on our images (Colaço et al. 2007; De Busserolles et al. 2009; Portail et al. 2018). Interestingly, the presence of microbial mats has been shown to be negatively correlated with the abundance of potential detritivores/grazers (Cuvelier et al. 2011a, 2017).

A few groups of small mussels (< 1 cm) were occasionally observed near the main mussel assemblage, possibly resulting from a recent recruitment event. In addition, large mussels with small individuals on their shells were observed in the permanent cover area, suggesting that this process contributes to the migration of small recruits and juveniles to areas of optimal environmental conditions (Van Dover et al. 1996). However, the resolution of our camera was insufficient to allow for the quantification of recruits on the substratum or mussel shells. Negative interactions, such as competition for space and resources, but also larviphagy and smothering, may contribute to the size segregation observed in hydrothermal mussel assemblages and may explain the rarity of smaller mussels in large mussel patches (Colaço et al. 1998; Lenihan et al. 2008). This type of negative interaction was corroborated by the arrival of a large mussel individual that caused the rapid departure of an entire patch of small mussels (i.e. < 5 mm), suggesting that larger mussels, with high mobility, may have a competitive advantage to access resources and occupy space. As observed in dense coastal mussel assemblages, these negative interactions may counterbalance the benefits of living in aggregation (Woodin 1974; Bertness and Grosholz 1985; Okamura 1986; Khaitov 2013). Although imagery has the potential to assess the role of recruitment and growth, the observed decadal stability did not allow the description of these processes.

Positive interactions also occurred in the studied assemblages. EOF analyses suggested a strong correlation between mat and mussel dynamics that may be due to facilitation processes. The migration of *B. azoricus* individuals may help to clear suitable habitats for microbial mats. Their development may also be facilitated by the remaining byssus that create new, complex colonisation surfaces. Moreover, the lateral dispersion of the hydrothermal fluid by mussels, which extends the available redox conditions, may also contribute to locally enhance the growth of microbial communities (Johnson et al. 1994; Crépeau et al. 2011). Heterotrophic microorganisms found in these mats (Crépeau et al. 2011) may benefit from the particulate and dissolved organic material found in higher concentrations in the mussel assemblage (Sarradin et al. 1999; review in Govenar 2012). Although microbial mats do not appear to affect the fitness of mussels on which they grow (Martins et al. 2009), they may contribute to the environmental transmission of symbionts (Crépeau et al. 2011). Finally, the affinity of microbial mats for mussel assemblages support the role of these mussels as a foundation species (Rybakova and Galkin 2015).

4.5. Comparisons with intertidal mussel assemblages

In the present study, the major scales of variation detected were infra-annual, mainly related to tidal forcing, but also to a few aperiodic events linked to very localised changes in environmental conditions. This is comparable, albeit to a lesser extent, to what is observed in intertidal areas where tidal variability involves periodic variation in exposure to stressors and nutrients (Connell 1961; Suchanek 1978; Johnson et al. 1994; Nedoncelle et al. 2015). As a result both intertidal and vent species developed adaptation to cope with fluctuations of environmental conditions such as hypoxia (Intertidal: Newell 1973; McMahon 1988a – Hydrothermal: Hourdez and Lallier 2007; Hourdez and Jollivet 2020; Le Layec and Hourdez 2021). A review of the different environmental forcings acting on mussel assemblages at LS,

but also in intertidal zones suggests a higher intensity of environmental stressors in the latter (e.g. wave action, air exposure; Table 4). In intertidal zones, the main source of variability results from exchanges at the air/water interface and direct sun exposure, while in the deep sea, the temperature of bottom seawater is relatively buffered from any source of climate disturbance. This may be different at vents where tide-related shifts in currents may initiate changes in fluid exposure for vent fauna (Nedoncelle et al. 2015; Lelièvre et al. 2017). For example, at diffuse-flow vents, tides may dictate most of the habitat variability in the short term with temperature variations limited to only a few degrees 10 to 30 centimetre away from the fluid exit (Sarrazin et al. 2014; Lee et al. 2015; Lelièvre et al. 2017). At high intertidal zones, tidal variability can be associated with large temperature gradients inducing mortality notably during extreme events caused by seasonality (Nakamura 1976; Dethier 1984). Predation also appears to have greater impact on intertidal mussels than those at vents (Table 4), because multiple coastal species including crabs, whelks and seabirds are potential predators (Okamura 1986; Hilgerloh et al. 1997; Hunt and Scheibling 1998, 2001).

Moreover, extreme events such as storms can cause major mussel dislodgement and mortality events in the intertidal zone, creating large gaps in the assemblages (Sousa 1979; Paine and Levin 1981; Witman 1987; Dayton et al. 1989) or even in non-sheltered mussel population over kilometres (Nehls and Thiel 1993; Table 4). Furthermore, centennial storms and earthquakes can severely alter the habitat by shaping the coastal geomorphology (Dayton et al. 1989; Castilla et al. 2010). Significant environmental variability at vents may result from aperiodic changes in subsurface hydrothermal circulation, structure collapses and from volcanic and tectonic events (Table 4). If relocation of the fluid exit is relatively progressive and occurring over small scales, mobility is an ecological asset to relocate in suitable conditions (Govenar et al. 2004; Copley et al. 2007; Bates et al. 2010; Sen et al. 2014). However, in the case of larger-scale event, recolonisation by migration may be limited by specific mobility capabilities.

Dramatic large-scale changes such as eruptions have been observed at vents, particularly at faster spreading ridges such as the East Pacific Rise or Juan de Fuca Ridge. These events, more common on fast spreading ridges, can eradicate the entire community back to the first colonisation stages (Tunnicliffe et al. 1997; Shank et al. 1998, 2003; Marcus et al. 2009). However, in this study, no such major event was observed during 7 years of investigation, neither at the local nor at the field scale. In fact, despite the limited spatial extent in our study, our repeated visits at LS indicate not only that the described stability was visually consistent over the entire studied edifice, but also, at the field scale, only a few sites have exhibited significant changes within the last 10 years.

Extreme events appear to be more frequent and intense in coastal areas compared with slow-spreading vent ecosystems where environmental variability is very low. Intertidal zones are particularly exposed during winter and summer, which are characterised by destructive storms, ice scouring or algal blooms (Table 4). Regarding the MAR, volcanic events are extremely rare (e.g. LS; Dziak et al. 2004; Ballu et al. 2019), although they may occur at a decadal frequency on faster-spreading ridges (review in Desbruyères 1998; Shank et al. 1998; review in Glover et al. 2010). This relative stability at slow-spreading ridges, questions the assumption that vent communities are exposed to extreme and highly variable conditions. It is obvious that vent ecosystem dynamics strongly contrast with that of the vast aperiodic and homogeneous surrounding deep sea, but our observations show that, at least at LS, mussel assemblages appear to experience relatively stable, clement and predictable conditions compared with their fast-spreading and coastal counterparts. That regime of infrequent and non-destructive disturbances can have important ecological implications. For example, under the “intermediate disturbance hypothesis” (Connell 1978), this regime may contribute to the lower diversity of the MAR vent fields previously attributed to higher isolation likelihood of slow-spreading system (review in Juniper and Tunnicliffe 1997; Van Dover and Trask 2000; Van Dover and Doerries 2005).

Table 4 – Abiotic and biotic conditions affecting the dynamics of mussel assemblages in the intertidal and hydrothermal environments. Not affected (-), affected (+; behavioural response, influence on few individuals only), strongly affected (++; > decimetre-scale influence in assemblages).

Source of influence	Process involved	Effect	
		Intertidal	Hydrothermal
Environmental			
<i>Infra-daily</i>			
Tides	Predictable changes	++	+
	Hydrodynamics & tidal variation	Desiccation/Temperature stress¹ 11, 22, 38, 43 Physical disturbance (log/boulder drift, waves)^{2, 3, 18, 21, 28, 56}	Changes in the distribution of the hydrothermal fluid carrying stressors and trophic resources 23, 65, 66, 61, 70, 72
<i>Infra-annual</i>			
Substratum instability		Little investigated	++ Structural collapse^{23, 36} Activation/deactivation of fluid outflow^{36, 60, 67}
Season	Storms	++	+
	Disturbance on hydrodynamics	Water velocity^{3, 13, 16, 18, 25, 26, 40}	Bottom pressure, current velocity^{24, 30, 70}
	Climate extremes	++	-
	Disturbance linked to winter ice and high/low temperatures	Physical dislodgement (e.g. ice scouring) and/or extreme environmental conditions 11, 17, 18, 33, 34, 44, 52, 53	Our data suggest high stability of the background deep-sea environment
	Life-history trait	+	+
	Spawning induction	<i>Mytilus edulis</i> spawns seasonally ⁷	Seasonal spawning of all species of

15, 31 *Bathymodiolus*^{42, 50, 51} except *B. thermophilus*⁷¹
Mytilus californianus: spawns continuously¹²

Decadal and more

Magmatic event	Eruption, earthquake	-	++
		<i>Not necessarily an intertidal feature. Few cases with mortality</i> ⁵⁷	<i>Fauna removal at medium to fast-spreading ridges</i> ⁵⁹
Long-term habitat change	Habitat suitability decline	++ Sanding up ⁵⁸	++ Waning ^{47, 62, 67, 68} Landslide ³⁶

Biotic

Predation		++	-/+
		Interspecific ^{3, 6, 9, 10, 11, 16, 27, 29, 32, 35, 39, 40}	Interspecific ^{45, 48, 49, 69, 63, 73} Larviphagy ⁵⁴
Competition for space/resources		++	++
		Interspecific ^{1, 3, 4, 5, 9, 11} Intraspecific ^{19, 27}	Interspecific ^{36, 41, 55, 67}
Recolonisation		++	++
		Recruitment ^{27, 64} Passive/active displacement ^{16, 27}	Recruitment ^{37, 41} Active displacement ^{67, 69}

Connell 1. 1961, 2. 1985; 3. Dayton 1971; 4. Harger 1972; Paine 5. 1974, 6. 1976; 7. Wilson and Seed 1974; 8. Woodin 1974; 9. Menge and Sutherland 1976; 10. Menge 1978; Suchanek 11. 1978, 12. 1981; Sousa 13. 1979, 14. 1984; 15. Pieters et al. 1980; 16. Paine and Levin 1981; 17. Tsuchiya 1983; 18. Dethier 1984; 19. Bertness and Grosholz 1985; 20. Okamura 1986; 21. Denny 1987; 22. McMahon 1988b; 23. Tunnicliffe and Juniper 1990; 24. Cannon et al. 1991; 25. McGrorty and Goss-Custard 1993; 26. Nehls and Thiel 1993; Wootton 27. 1993, 28. 2001; 29. Petraitis 1995; 30. Cannon and Thomson 1996; 31. Gray et al. 1997; 32. Hilgerloh et al. 1997; 33. McCook and Chapman 1997; 34. Minchinton et al. 1997; 35. Nehls et al. 1997; 36. Sarrazin et al. 1997; 37. Comtet and Desbruyeres 1998; 38. Denny and Paine 1998; Hunt and Scheibling 39. 1998, 40. 2001; 41. Shank et al. 1998; 42. review in Tyler and Young 1999; 43. Denny and Wethey 2001; 44. Strasser et al. 2001; 45.

Micheli et al. 2002; 46. Mullineaux et al. 2003; 47. Tsurumi and Tunnicliffe 2003; 48. Urcuyo et al. 2003; 49. Sancho et al. 2005; 50. Colaço et al. 2006; 51. Dixon et al. 2006; 52. Steenbergen et al. 2006; 53. Beukema and Dekker 2007; 54. Lenihan et al. 2008; 55. Lutz et al. 2008; 56. van De Koppel et al. 2008; 57. Castilla et al. 2010; 58. Dolch and Reise 2010; 59. review in Glover et al. 2010; Cuvelier et al. 60. 2011b, 61. 2014; 62. Fabri et al. 2011; 63. Govenar 2012; 64. Khaitov 2013; Nedoncelle et al. 65. 2013, 66. 2015; Sen et al. 67. 2014, 68. 2016; 69. Matabos et al. 2015; 70. Lelièvre et al. 2017; 71. review in Laming et al. 2018; 72. Mat et al. 2020; 73. Marticorena et al. 2021

Conclusion

Our results showed that faunal dynamics within the studied vent assemblage varied with changes in the local physico-chemical conditions at the decimetre scale. Moreover, as hypothesised in other studies (Sarrazin et al. 1997, 2002), substratum properties (e.g. maturation stage in terms of friability, porosity, mineralogy) can constrain the distribution of species, especially in more variable habitats such as the immediate vicinity of vent orifices. Imagery data, although limited to a few visible taxa, allowed us to characterise and confirm a few biotic processes or interactions. We confirmed the role of *B. azoricus* as a foundation species, providing a habitat to a variety of associated species, transporting smaller individuals and facilitating the installation of microbial mats through habitat modifications. Larger mussels can migrate in response to environmental changes, as previously suggested by several authors. The role of this mobility in the local dynamics of vent assemblages must be considered, although it had no significant effect on the studied assemblage. Other observations, such as the displacement of individual mussels, needs further attention. The negligible role of predation on mature mussel individuals was supported by the absence of significant mortality over the study period. However, this process may be more important during the first colonisation stages: a single observation of a competitive relationship between large and small mussels lends support to this assumption. To conclude, the observations made in the present study were insufficient to support our hypothesis (H6) on the significant influence of biological interactions on

assemblage dynamics. Further investigations on the role of these interactions on the fate of hydrothermal assemblages are required. Manipulative experiments on the seafloor, such as predator exclusion or recruitment studies may hold the key to obtaining some answers. Overall, this unprecedented 7-year daily imagery time-series reveals a high stability in vent assemblage in terms of fluid discharge, species distribution and the absence of major growth or recruitment. These results questions the assumption that, at least along the slow-spreading centres of the MAR, vent communities are highly dynamic and exposed to extreme and highly variable conditions.

Data availability statement

Data used in this are available on the EMSO-Azores platform: <https://www.emso-fr.org/EMSO-Azores> and stored in the SEANOE database. Individual DOIs of the MoMARSAT cruises from 2011 to 2019 can be found within the general DOI of “MoMARSAT: Monitoring the Mid-Atlantic Ridge” 10.18142/130. *Note to the editor and reviewers: A link to all data will be provided before publication, the files are being currently processed to be assigned a DOI.*

Authors' contribution

JS and MM conceived this study. JS, PMS and AL participated in the development of the TEMPO ecological & environmental modules and the EMSO-Azores observatory. LVA, MM and JD performed image analyses. AL processed sulphide and iron concentrations data acquired with the CHEMINI chemical analysers. ABA and LVA carried out statistical analyses. LVA, MM and JS interpreted the data and drafted the manuscript. All co-authors reviewed the manuscript.

Acknowledgments

We warmly thank the crews of the R/Vs *Pourquoi pas?*, *L'Atalante* and *Thalassa* and pilots of the HOV *Nautille* and ROV *Victor6000* submersibles who have participated in the MoMARSAT cruises since 2010 (<https://doi.org/10.18142/130>). We acknowledge P.-M. Sarradin and M. Cannat for co-leading and managing the MoMARSAT cruises and the EMSO-Azores observatory. We are grateful to the engineers and technicians from the RDT and LEP research labs at the IFREMER REM department for the development and on-board maintenance of the TEMPO ecological module and the SeaMON East node, the development and maintenance of *in situ* chemical analysers, and support with instrumentation at sea. The EMSO-Azores observatory has been set up for over a decade; we gratefully thank anyone who has contributed

to this research. We acknowledge the work of interns V. Courant, E. Jaulin, L. Le Goffic and C. Raffault who helped for image annotation. We are grateful to three anonymous reviewers who improved considerably the quality of this article. This manuscript was professionally edited by C. Engel-Gautier.

This work and LVA's PhD thesis were supported by the European Union's Horizon 2020 research and innovation project iAtlantic under Grant Agreement No. 818123. We also acknowledge financial support from the EU project EMSO (<http://www.emso-eu.org/>) and the French observatory EMSO-Azores funded by IFREMER and CNRS.

The authors declare that the research was conducted in the absence of any commercial or financial relationships that could be construed as a potential conflict of interest.

References

- Agarwal, A., C. V. Jawahar, and P. J. Narayanan. 2005. A survey of planar homography estimation techniques. Tech. Rep. IIIT/TR/2005/12 1–25.
- Aron, M., D. Cuvelier, J. Aguzzi, C. Costa, C. Doya, J. Sarrazin, and P. M. Sarradin. 2013. Preliminary results on automated video-imaging for the study of behavioural rhythms of tubeworms from the TEMPO-mini ecological module (NEPTUNE, Canada). *Martech 2013 5th International Workshop on Marine Technology. SARTI*. 35–37.
- Ballu, V., T. Barreyre, M. Cannat, L. Testut, W. Crawford, J. Escartín, T. Coulombier, and V. Chavagnac. 2019. What happened in 2015 at the Lucky Strike volcano? *Geophys. Res. Abstr.* **21**.
- Barreyre, T., J. Escartín, R. Garcia, M. Cannat, E. Mittelstaedt, and R. Prados. 2012. Structure, temporal evolution, and heat flux estimates from the Lucky Strike deep-sea hydrothermal field derived from seafloor image mosaics. *Geochemistry, Geophys. Geosystems* **13**: 1–29. doi:10.1029/2011GC003990
- Barreyre, T., J. Escartín, R. A. Sohn, M. Cannat, V. Ballu, and W. C. Crawford. 2014. Temporal variability and tidal modulation of hydrothermal exit-fluid temperatures at the Lucky Strike deep-sea vent field, Mid-Atlantic Ridge. *J. Geophys. Res. Solid Earth* **119**: 2543–2566. doi:10.1002/2015JB012608. Received
- Bates, A. E., R. W. Lee, V. Tunnicliffe, and M. D. Lamare. 2010. Deep-sea hydrothermal vent animals seek cool fluids in a highly variable thermal environment. *Nat. Commun.* **1**: 1–6. doi:10.1038/ncomms1014
- Bay, H., T. Tuytelaars, and L. Van Gool. 2006. SURF: Speeded Up Robust Features. *Comput. Vision–ECCV 2006 Part I*: 404–417.

- Bertness, M. D., and E. Grosholz. 1985. Population Dynamics of the Ribbed Mussel ,
Geukensia demissa : The Costs and Benefits of an Aggregated Distribution. *Oecologia*
67: 192–204. doi:<https://www.jstor.org/stable/4217712>
- Beukema, J. J., and R. Dekker. 2007. Variability in annual recruitment success as a
determinant of long-term and large-scale variation in annual production of intertidal
Wadden Sea mussels (*Mytilus edulis*). *Helgol. Mar. Res.* **61**: 71–86.
doi:[10.1007/s10152-006-0054-3](https://doi.org/10.1007/s10152-006-0054-3)
- Blandin, J., A. Colaco, J. Legrand, M. Cannat, P.-M. Sarradin, and J. Sarrazin. 2010. The
MoMAR-D project : a challenge to monitor in real time the Lucky Strike hydrothermal
vent field. *ICES J. Mar. Sci.* **68**: 416–424.
- Bougerol, M., I. Boutet, D. LeGuen, D. Jollivet, and A. Tanguy. 2015. Transcriptomic
response of the hydrothermal mussel *Bathymodiolus azoricus* in experimental exposure
to heavy metals is modulated by the Pgm genotype and symbiont content. *Mar.*
Genomics **21**: 63–73. doi:[10.1016/j.margen.2014.11.010](https://doi.org/10.1016/j.margen.2014.11.010)
- Boutet, I., A. Tanguy, D. Le Guen, P. Piccino, S. Hourdez, P. Legendre, and D. Jollivet. 2009.
Global depression in gene expression as a response to rapid thermal changes in vent
mussels. *Proc. R. Soc. B Biol. Sci.* **276**: 3071–3079. doi:[10.1098/rspb.2009.0503](https://doi.org/10.1098/rspb.2009.0503)
- Le Bris, N., B. Govenar, C. Le Gall, and C. R. Fisher. 2006. Variability of physico-chemical
conditions in 9°50'N EPR diffuse flow vent habitats. *Mar. Chem.* **98**: 167–182.
doi:[10.1016/j.marchem.2005.08.008](https://doi.org/10.1016/j.marchem.2005.08.008)
- Britayev, T. A., D. Martin, E. M. Krylova, R. Von Cosel, and T. S. Aksiuk. 2007. Life-history
traits of the symbiotic scale-worm *Branchiopolynoe seepensis* and its relationships with
host mussels of the genus *Bathymodiolus* from hydrothermal vents. *Mar. Ecol.* **28**: 36–
48. doi:[10.1111/j.1439-0485.2007.00152.x](https://doi.org/10.1111/j.1439-0485.2007.00152.x)

- De Busserolles, F., J. Sarrazin, O. Gauthier, Y. Gélinas, M. C. Fabri, P. M. Sarradin, and D. Desbruyères. 2009. Are spatial variations in the diets of hydrothermal fauna linked to local environmental conditions? *Deep. Res. Part II Top. Stud. Oceanogr.* **56**: 1649–1664. doi:10.1016/j.dsr2.2009.05.011
- Cannat, M., A. Briaies, C. Deplus, and others. 1999. Mid-Atlantic Ridge – Azores hotspot interactions : along-axis migration of a hotspot-derived event of enhanced magmatism 10 to 4 Ma ago. **173**: 257–269.
- Cannat, M., P.-M. Sarradin, J. Blandin, J. Escartin, and A. Colaço. 2011. MoMar-Demo at Lucky Strike. A near-real time multidisciplinary observatory of hydrothermal processes and ecosystems at the Mid-Atlantic Ridge. *In: A.G.U. Fall Meeting, Abstract OS22A-05, San Francisco.*
- Cannat, M., P. Sarradin, J. Blandin, and others. 2016. EMSO-Azores : Monitoring seafloor and water column processes at the Mid-Atlantic Ridge. Fix03-Project Newsletter. Sevice Act. Spec. **3**: 16–17.
- Cannon, G. A., D. J. Pashinski, and M. R. Lemon. 1991. Middepth Flow Near Hydrothermal Venting Sites on the Southern Juan de Fuca Ridge. *J. Geophys. Res.* **96**: 12815–12831.
- Cannon, G. A., and R. E. Thomson. 1996. Characteristics of 4-day oscillations trapped by the Juan de Fuca Ridge. *Geophys. Res. Lett.* **23**: 1613–1616.
- Castilla, J. C., P. H. Manríquez, and A. Camaño. 2010. Effects of rocky shore coseismic uplift and the 2010 Chilean mega-earthquake on intertidal biomarker species. *Mar. Ecol. Prog. Ser.* **418**: 17–23. doi:10.3354/meps08830
- Charlou, J. L., J. P. Donval, E. Douville, P. Jean-Baptiste, J. Radford-Knoery, Y. Fouquet, A. Dapoigny, and M. Stievenard. 2000. Compared geochemical signatures and the evolution

- of Menlimnez Gwen (37°50' N) and Lucky Strike (37°17' N) hydrothermal fluids, south of the Azores Triple Junction on the Mid-Atlantic Ridge. *Chem. Geol.* **171**: 49–75.
- Chavagnac, V., T. Leleu, F. Fontaine, M. Cannat, G. Ceuleneer, and A. Castillo. 2018. Spatial Variations in Vent Chemistry at the Lucky Strike Hydrothermal Field, Mid-Atlantic Ridge (37°N): Updates for Subseafloor Flow Geometry From the Newly Discovered Capelinhos Vent. *Geochemistry, Geophys. Geosystems* **19**: 4444–4458.
doi:10.1029/2018GC007765
- Chevaldonné, P., D. Desbruyères, and M. Le Haître. 1991. Time-series of temperature from three deep-sea hydrothermal vent sites. *Deep Sea Res. Part A, Oceanogr. Res. Pap.* **38**: 1417–1430.
- Childress, J. J. 1988. Biology and chemistry of a deep-sea hydrothermal vent on the Galapagos Rift; the Rose Garden in 1985. Introduction. *Deep Sea Res. Part A, Oceanogr. Res. Pap.* **35**: 1677–1680. doi:10.1016/0198-0149(88)90043-X
- Childress, J. J., and C. R. Fisher. 1992. The biology of hydrothermal vent animals: physiology, biochemistry and autotrophic symbioses., p. 337–441. *In* M. Barnes, A.D. Ansell, and R.N. Gibson [eds.], *Oceanography and Marine Biology Annual Review*. UCL Press.
- Colaço, A., F. Dehairs, and D. Desbruyères. 2002. Nutritional relations of deep-sea hydrothermal fields at the Mid-Atlantic Ridge: A stable isotope approach. *Deep. Res. Part I Oceanogr. Res. Pap.* **49**: 395–412. doi:10.1016/S0967-0637(01)00060-7
- Colaço, A., D. Desbruyères, T. Comtet, and A. M. Alayse. 1998. Ecology of the Menez Gwen hydrothermal vent field (Mid-Atlantic Ridge/Azores Triple Junction). *Cah. Biol. Mar.* **39**: 237–240.

- Colaço, A., D. Desbruyères, and J. Guezennec. 2007. Polar lipid fatty acids as indicators of trophic associations in a deep-sea vent system community. *Mar. Ecol.* **28**: 15–24.
doi:10.1111/j.1439-0485.2006.00123.x
- Colaço, A., I. Martins, M. Laranjo, and others. 2006. Annual spawning of the hydrothermal vent mussel, *Bathymodiolus azoricus*, under controlled aquarium, conditions at atmospheric pressure. *J. Exp. Mar. Bio. Ecol.* **333**: 166–171.
doi:10.1016/j.jembe.2005.12.005
- Company, R., A. Serafim, R. Cosson, A. Fiala-Médioni, D. Dixon, and M. João Bebianno. 2006. Temporal variation in the antioxidant defence system and lipid peroxidation in the gills and mantle of hydrothermal vent mussel *Bathymodiolus azoricus*. *Deep. Res. Part I Oceanogr. Res. Pap.* **53**: 1101–1116. doi:10.1016/j.dsr.2006.05.008
- Comtet, T., and D. Desbruyères. 1998. Population structure and recruitment in mytilid bivalves from the Lucky Strike and Menez Gwen on the Mid-Atlantic Ridge). *Ecology* **163**: 165–177.
- Connell, J. H. 1961. The Influence of Interspecific Competition and Other Factors on the Distribution of the Barnacle *Chthamalus Stellatus*. *Ecology* **42**: 710–723.
- Connell, J. H. 1978. Diversity in Tropical Rain Forests and Coral Reefs. *Science (80-.)*. **199**: 1302–1310.
- Connell, J. H. 1985. The consequences of variation in initial settlement vs. post-settlement mortality in rocky intertidal communities. *J. Exp. Mar. Bio. Ecol.* **93**: 11–45.
doi:10.1016/0022-0981(85)90146-7
- Copley, J. T. P., P. B. K. Jorgensen, and R. A. Sohn. 2007. Assessment of decadal-scale ecological change at a deep Mid-Atlantic hydrothermal vent and reproductive time-series

- in the shrimp *Rimicaris exoculata*. *J. Mar. Biol. Assoc. United Kingdom* **95**: 1–3.
doi:10.1017/S0025315414001738
- Crépeau, V., M. A. Cambon Bonavita, F. Lesongeur, H. Randrianalivelo, P. M. Sarradin, J. Sarrazin, and A. Godfroy. 2011. Diversity and function in microbial mats from the Lucky Strike hydrothermal vent field. *FEMS Microbiol. Ecol.* **76**: 524–540.
doi:10.1111/j.1574-6941.2011.01070.x
- Crone, T. J., and W. S. D. Wilcock. 2005. Modeling the effects of tidal loading on mid-ocean ridge hydrothermal systems. *Geochemistry, Geophys. Geosystems* **6**: 25.
doi:10.1029/2004GC000905
- Cuvelier, D., P. Legendre, A. Laës-Huon, P. M. Sarradin, and J. Sarrazin. 2017. Biological and environmental rhythms in (dark) deep-sea hydrothermal ecosystems. *Biogeosciences* **14**: 2955–2977. doi:10.5194/bg-14-2955-2017
- Cuvelier, D., P. Legendre, A. Laes, P.-M. Sarradin, and J. Sarrazin. 2014. Rhythms and community dynamics of a hydrothermal tubeworm assemblage at main endeavour field - A multidisciplinary deep-sea observatory approach. *PLoS One* **9**.
doi:10.1371/journal.pone.0096924
- Cuvelier, D., P.-M. Sarradin, J. Sarrazin, and others. 2011a. Hydrothermal faunal assemblages and habitat characterisation at the Eiffel Tower edifice (Lucky Strike, Mid-Atlantic Ridge). *Mar. Ecol.* **32**: 243–255. doi:10.1111/j.1439-0485.2010.00431.x
- Cuvelier, D., J. Sarrazin, A. Colaço, J. Copley, D. Desbruyères, A. G. Glover, P. Tyler, and R. Serrão Santos. 2009. Distribution and spatial variation of hydrothermal faunal assemblages at Lucky Strike (Mid-Atlantic Ridge) revealed by high-resolution video image analysis. *Deep. Res. Part I Oceanogr. Res. Pap.* **56**: 2026–2040.
doi:10.1016/j.dsr.2009.06.006

- Cuvelier, D., J. Sarrazin, A. Colaço, J. T. Copley, A. G. Glover, P. A. Tyler, R. S. Santos, and D. Desbruyères. 2011b. Community dynamics over 14 years at the Eiffel Tower hydrothermal edifice on the Mid-Atlantic Ridge. *Limnol. Oceanogr.* **56**: 1624–1640. doi:10.4319/lo.2011.56.5.1624
- d'Angelo, P. 2005. Hugin-Panorama photo stitcher. Sourceforge.
- Von Damm, K. L., A. M. Bray, L. G. Buttermore, and S. E. Oosting. 1998. The geochemical controls on vent fluids from the Lucky Strike vent field, Mid-Atlantic Ridge. *Earth Planet. Sci. Lett.* **160**: 521–536. doi:10.1016/S0012-821X(98)00108-3
- Davis, E., and K. Becker. 1999. Tidal pumping of fluids within and from the oceanic crust: New observations and opportunities for sampling the crustal hydrosphere. *Earth Planet. Sci. Lett.* **172**: 141–149. doi:10.1016/S0012-821X(99)00197-1
- Dayton, P. K. 1971. Competition, Disturbance, and Community Organization : The Provision and Subsequent Utilization of Space in a Rocky Intertidal Community. *Ecol. Monogr.* **41**: 351–389.
- Dayton, P. K., M. J. Tegner, R. J. Seymour, and P. E. Parnell. 1989. Unusual County Marine Erosion in San Diego from a Single Storm. *Estuar. Coast. Shelf Sci.* **29**: 151–160.
- Demina, L. L., and S. V. Galkin. 2008. On the role of abiogenic factors in the bioaccumulation of heavy metals by the hydrothermal fauna of the Mid-Atlantic Ridge. *Oceanology* **48**: 784–797. doi:10.1134/S0001437008060040
- Denny, M. W. 1987. Lift as a mechanism of patch initiation in mussel beds. *J. Exp. Mar. Bio. Ecol.* **113**: 231–245. doi:10.1016/0022-0981(87)90103-1
- Denny, M. W., and R. T. Paine. 1998. Celestial mechanics, sea-level changes, and intertidal ecology. *Biol. Bull.* **194**: 108–115. doi:10.2307/1543040

- Denny, M. W., and D. Wethey. 2001. Physical processes that generate patterns in marine communities. *Mar. Community Ecol.* 3–37.
- Desbruyères, D. 1998. Temporal variations in the vent communities on the East Pacific Rise and Galapagos Spreading Centre: A review of present knowledge. *Cah. Biol. Mar.* **39**: 241–244.
- Desbruyères, D., M. Biscoito, J. C. Caprais, and others. 2001. Variations in deep-sea hydrothermal vent communities on the Mid-Atlantic Ridge near the Azores plateau. *Deep. Res. Part I Oceanogr. Res. Pap.* **48**: 1325–1346. doi:10.1016/S0967-0637(00)00083-2
- Dethier, M. N. 1984. Disturbance and Recovery in Intertidal Pools : Maintenance of Mosaic Patterns. *Ecol. Monogr.* **54**: 99–118.
- Dixon, D. R., D. M. O. Lowe, P. I. O. Miller, G. R. Villemin, A. Colac, and R. Serra. 2006. Evidence of seasonal reproduction in the Atlantic vent mussel *Bathymodiolus azoricus* , and an apparent link with the timing of photosynthetic primary production. *J. Mar. Biol. Assoc. United Kingdom* **86**: 1363–1371. doi:10.1017/S0025315406014391
- Dolch, T., and K. Reise. 2010. Long-term displacement of intertidal seagrass and mussel beds by expanding large sandy bedforms in the northern Wadden Sea. *J. Sea Res.* **63**: 93–101. doi:10.1016/j.seares.2009.10.004
- Van Dover, C. L., D. Desbruyères, M. Segonzac, T. Comtet, L. Saldanha, A. Fiala-Médioni, and C. Langmuir. 1996. Biology of the Lucky Strike hydrothermal field. *Deep. Res. Part I Oceanogr. Res. Pap.* **43**: 1509–1529. doi:10.1016/S0967-0637(96)00051-9
- Van Dover, C. L., and M. B. Doerries. 2005. Community structure in mussel beds at Logatchev hydrothermal vents and a comparison of macrofaunal species richness on

- slow- and fast-spreading mid-ocean ridges. *Mar. Ecol.* **26**: 110–120. doi:10.1111/j.1439-0485.2005.00047.x
- Van Dover, C. L., and J. L. Trask. 2000. Diversity at deep-sea hydrothermal vent and intertidal mussel beds. *Mar. Ecol. Prog. Ser.* **195**: 169–178. doi:10.3354/meps195169
- Duperron, S., C. Bergin, F. Zielinski, and others. 2006. A dual symbiosis shared by two mussel species, *Bathymodiolus azoricus* and *Bathymodiolus puteoserpentis* (Bivalvia: Mytilidae), from hydrothermal vents along the northern Mid-Atlantic Ridge. *Environ. Microbiol.* **8**: 1441–1447. doi:10.1111/j.1462-2920.2006.01038.x
- Dziak, R. P., D. K. Smith, D. W. R. Bohnenstiehl, C. G. Fox, D. Desbruyeres, H. Matsumoto, M. Tolstoy, and D. J. Fornari. 2004. Evidence of a recent magma dike intrusion at the slow spreading Lucky Strike segment, Mid-Atlantic Ridge. *J. Geophys. Res. Solid Earth* **109**: 1–15. doi:10.1029/2004JB003141
- Erickson, K. L., S. A. Macko, and C. L. Van Dover. 2009. Evidence for a chemoautotrophically based food web at inactive hydrothermal vents (Manus Basin). *Deep. Res. Part II* **56**: 1577–1585. doi:10.1016/j.dsr2.2009.05.002
- Fabri, M. C., A. Bargain, P. Briand, A. Gebruk, Y. Fouquet, M. Morineaux, and D. Desbruyeres. 2011. The hydrothermal vent community of a new deep-sea field, Ashadze-1, 12°58'N on the Mid-Atlantic Ridge. *J. Mar. Biol. Assoc. United Kingdom* **91**: 1–13. doi:10.1017/S0025315410000731
- Ferreira, T., and W. Rasband. 2012. The ImageJ 1.44 User Guide. *ImageJ/Fiji* 131–134.
- Fiala-Médioni, A., Z. P. McKiness, P. Dando, J. Boulegue, A. Mariotti, A. M. Alayse-Danet, J. J. Robinson, and C. M. Cavanaugh. 2002. Ultrastructural, biochemical, and immunological characterization of two populations of the mytilid mussel *Bathymodiolus*

- azoricus from the Mid-Atlantic Ridge: Evidence for a dual symbiosis. *Mar. Biol.* **141**: 1035–1043. doi:10.1007/s00227-002-0903-9
- Fornari, D. J., T. Shank, K. L. Von Damm, and others. 1998. Time-series temperature measurements at high-temperature hydrothermal vents, East Pacific Rise 9°49'–51'N: Evidence for monitoring a crustal cracking event. *Earth Planet. Sci. Lett.* **160**: 419–431. doi:10.1016/S0012-821X(98)00101-0
- Fouquet, Y., J.-L. Charlou, I. Costa, and others. 1994. A detailed study of the Lucky Strike hydrothermal site discovery of a new hydrothermal site: Menez Gwen; preliminary results of the DIVA1 cruise [5–29 May 1994]. *InterRidge News* **3**: 14–17.
- Fustec, A., D. Desbruyères, and S. K. Juniper. 1987. Deep-Sea Hydrothermal Vent Communities at 13 ° N on the East Pacific Rise : Microdistribution and Temporal Variations. *Biol. Oceanogr.* **4**: 121–164. doi:10.1080/01965581.1987.10749487
- Girard, F., J. Sarrazin, A. Arnaubec, M. Cannat, P.-M. Sarradin, B. Wheeler, and M. Matabos. 2020. Currents and topography drive assemblage distribution on an active hydrothermal edifice. *Prog. Oceanogr.* **187**: 102397. doi:10.1016/j.pocean.2020.102397
- Glover, A. G., A. J. Gooday, D. M. Bailey, and others. 2010. Temporal Change in Deep-Sea Benthic Ecosystems. A Review of the Evidence From Recent Time-Series Studies,.
- Goffredi, S. K., C. Motooka, D. A. Fike, L. C. Gusmão, E. Tilic, G. W. Rouse, and E. Rodríguez. 2021. Mixotrophic chemosynthesis in a deep-sea anemone from hydrothermal vents in the Pescadero Basin, Gulf of California. *BMC Biol.* **19**: 1–18. doi:10.1186/s12915-020-00921-1
- Gonzalez, A., R. M. Germain, D. S. Srivastava, and others. 2020. Scaling-up biodiversity-ecosystem functioning research. *Ecol. Lett.* **23**: 757–776. doi:10.1111/ele.13456

- Govenar, B. 2012. Energy transfer through food webs at hydrothermal vents linking the lithosphere to the biosphere. *Oceanography* **25**: 246–255. doi:10.5670/oceanog.2012.23
- Govenar, B., M. Freeman, D. C. Bergquist, G. A. Johnson, and C. R. Fisher. 2004. Composition of a one-year-old *Riftia pachyptila* community following a clearance experiment: Insight to succession patterns at deep-sea hydrothermal vents. *Biol. Bull.* **207**: 177–182. doi:10.2307/1543204
- Gray, A. P., R. Seed, and C. A. Richardson. 1997. Reproduction and growth of *Mytilus edulis chilensis* from the Falkland Islands. *Sci. Mar.* **61**: 39–48.
- Grelon, D., M. Morineaux, G. Desrosiers, and S. K. Juniper. 2006. Feeding and territorial behavior of *Paralvinella sulfincola*, a polychaete worm at deep-sea hydrothermal vents of the Northeast Pacific Ocean. *J. Exp. Mar. Bio. Ecol.* **329**: 174–186. doi:10.1016/j.jembe.2005.08.017
- Hannachi, A., I. T. Jolliffe, and D. B. Stephenson. 2007. Empirical orthogonal functions and related techniques in atmospheric science: A review. *Int. J. Climatol.* **27**: 1119–1152. doi:10.1002/joc
- Harger, J. R. W. 1972. Competitive coexistence: maintenance of interacting associations of the sea *Mytilus edulis* and *Mytilus californianus*. *Veliger* **14**: 387–410.
- Hilgerloh, G., M. Herlyn, and H. Michaelis. 1997. The influence of predation by herring gulls *Larus argentatus* and oystercatchers *Haematopus ostralegus* on a newly established mussel *Mytilus edulis* bed in autumn and winter. *Helgolander Meeresuntersuchungen* **51**: 173–189. doi:10.1007/BF02908706
- Hollander, M., and D. Wolfe. 1999. *Nonparametric statistical methods*, John Wiley & Sons.
- Hourdez, S., and D. Jollivet. 2020. Metazoan adaptation to deep-sea hydrothermal vents. *Life*

- Extrem. Environ. 42–67. doi:10.1017/9781108683319.004
- Hourdez, S., and F. H. Lallier. 2007. Adaptations to hypoxia in hydrothermal-vent and cold-seep invertebrates. *Rev. Environ. Sci. Biotechnol.* **6**: 143–159. doi:10.1007/s11157-006-9110-3
- Howse, J. 2013. *OpenCV Computer Vision with Python*, Packt Publishing Ltd.
- Humphris, S. E., D. J. Fornari, D. S. Scheirer, C. R. German, and L. M. Parson. 2002. Geotectonic setting of hydrothermal activity on the summit of Lucky Strike Seamount (37°17'N, Mid-Atlantic Ridge). *Geochemistry, Geophys. Geosystems* **3**: 2004.
- Hunt, H. L., and R. E. Scheibling. 1998. Effects of whelk (*Nucella lapillus* (L.)) predation on mussel (*Mytilus trossulus* (Gould), *M. edulis* (L.)) assemblages in tidepools and on emergent rock on a wave-exposed rocky shore in Nova Scotia, Canada. *J. Exp. Mar. Bio. Ecol.* **226**: 87–113. doi:10.1016/S0022-0981(97)00239-6
- Hunt, H. L., and R. E. Scheibling. 2001. Patch dynamics of mussels on rocky shores: integrating process to understand pattern. *Ecology* **82**: 3213–3231.
- Husson, B., P. M. Sarradin, D. Zeppilli, and J. Sarrazin. 2017. Picturing thermal niches and biomass of hydrothermal vent species. *Deep. Res. Part II* **137**: 6–25. doi:10.1016/j.dsr2.2016.05.028
- Jamieson, J. W., M. D. Hannington, M. K. Tivey, and others. 2016. Precipitation and growth of barite within hydrothermal vent deposits from the Endeavour Segment, Juan de Fuca Ridge. *Geochim. Cosmochim. Acta* **173**: 64–85. doi:10.1016/j.gca.2015.10.021
- Jannasch, H. W. 1985. Review Lecture-The chemosynthetic support of life and the microbial diversity at deep-sea hydrothermal vents. *Proc. R. Soc. London. Ser. B. Biol. Sci.* **225**: 277–297.

- João, M., C. Cardoso, T. Gomes, J. Blasco, R. Serrão, and A. Colaço. 2018. Metal interactions between the polychaete *Branchiopolynoe seepensis* and the mussel *Bathymodiolus azoricus* from Mid-Atlantic-Ridge hydrothermal vent fields. *Mar. Environ. Res.* **135**: 70–81. doi:10.1016/j.marenvres.2018.01.017
- Johnson, K. S., J. J. Childress, and C. L. Beehler. 1988a. Short-term temperature variability in the Rose Garden hydrothermal vent field : an unstable deep-sea environment. *Deep Sea Res.* **35**: 1711–1721.
- Johnson, K. S., J. J. Childress, C. L. Beehler, and C. M. Sakamoto. 1994. Biogeochemistry of hydrothermal vent mussel communities : the deep-sea analogue to the intertidal zone. *Deep. Res. I* **4**: 993–1011.
- Johnson, K. S., J. J. Childress, and R. R. Hessler. 1988b. Chemical and biological interactions in the Rose Garden hydrothermal vent field , Galapagos spreading center. *Deep Sea Res.* **35**: 1723–1744.
- Juniper, S. K., and V. Tunnicliffe. 1997. Crustal accretion and the hot vent ecosystem. *Philos. Trans. R. Soc. A Math. Phys. Eng. Sci.* **355**: 459–474. doi:10.1098/rsta.1997.0017
- Khaitov, V. 2013. Life in an unstable house : community dynamics in changing mussel beds. *Hydrobiologia* **706**: 139–158. doi:10.1007/s10750-012-1283-x
- Khripounoff, A., A. Vangriesheim, P. Crassous, M. Segonzac, V. Lafon, and A. Warén. 2008. Temporal variation of currents, particulate flux and organism supply at two deep-sea hydrothermal fields of the Azores Triple Junction. *Deep. Res. Part I Oceanogr. Res. Pap.* **55**: 532–551. doi:10.1016/j.dsr.2008.01.001
- van De Koppel, J., J. C. Gascoigne, G. Theraulaz, M. Rietkerk, W. M. Mooij, and P. M. J. Herman. 2008. Experimental evidence for spatial self-organization and its emergent

- effects in mussel bed ecosystems. *Science* (80-.). **322**: 739–742.
doi:10.1126/science.1163952
- Laes-Huon, A., C. Cathalot, J. Legrand, V. Tanguy, and P. M. Sarradin. 2016. Long-Term in situ survey of reactive iron concentrations at the Emso-Azores observatory. *IEEE J. Ocean. Eng.* **41**: 744–752. doi:10.1109/JOE.2016.2552779
- Laming, S. R., S. M. Gaudron, S. Duperron, and A. D. Rogers. 2018. Lifecycle Ecology of Deep-Sea Chemosymbiotic Mussels : A Review. **5**. doi:10.3389/fmars.2018.00282
- Langmuir, C., S. Humphris, D. Fornari, and others. 1997. Hydrothermal vents near a mantle hot spot: The Lucky Strike vent field at 37°N on the Mid-Atlantic Ridge. *Earth Planet. Sci. Lett.* **148**: 69–91. doi:10.1016/s0012-821x(97)00027-7
- Langmuir, C. L., J. L. Charlou, D. Colodner, and others. 1993. Lucky Strike-A newly discovered hydrothermal site on the Azores platform. *RIDGE Events* **4**: 3–5.
- Lantéri, N., H. A. Ruhl, A. Gates, and others. 2022. The EMSO Generic Instrument Module (EGIM): Standardized and Interoperable Instrumentation for Ocean Observation. *Front. Mar. Sci.* **9**: 1–17. doi:10.3389/fmars.2022.801033
- Le Layec, V., and S. Hourdez. 2021. Oxygen consumption rates in deep-sea hydrothermal vent scale worms: Effect of life-style, oxygen concentration, and temperature sensitivity. *Deep. Res. Part I Oceanogr. Res. Pap.* **172**: 103531. doi:10.1016/j.dsr.2021.103531
- Lee, R. W., K. Robert, M. Matabos, A. E. Bates, and S. K. Juniper. 2015. Temporal and spatial variation in temperature experienced by macrofauna at Main Endeavour hydrothermal vent field. *Deep. Res. Part I Oceanogr. Res. Pap.* **106**: 154–166.
doi:10.1016/j.dsr.2015.10.004
- Legendre, P. 2012. Whittaker-Robinson periodogram. *R Progr. Doc.*

- Legendre, P., and L. Legendre. 2012. Numerical ecology, Elsevier.
- Leleu, T., V. Chavagnac, M. Cannat, G. Ceuleneer, A. Castillo, and L. Menjot. 2015. Fluid geochemistry of the Capelinhos Vent Site. A Key to Understand the Lucky Strike Hydrothermal Vent Field (37°N, MAR). Am. Geophys. Union, Fall Meet. **abstract i**.
- Lelièvre, Y., P. Legendre, M. Matabos, S. Mihály, R. W. Lee, P. M. Sarradin, C. P. Arango, and J. Sarrazin. 2017. Astronomical and atmospheric impacts on deep-sea hydrothermal vent invertebrates. Proc. R. Soc. B Biol. Sci. **284**. doi:10.1098/rspb.2016.2123
- Lenihan, H. S., S. W. Mills, L. S. Mullineaux, C. H. Peterson, C. R. Fisher, and F. Micheli. 2008. Biotic interactions at hydrothermal vents : Recruitment inhibition by the mussel *Bathymodiolus thermophilus*. Deep. Res. I **55**: 1707–1717. doi:10.1016/j.dsr.2008.07.007
- Léveillé, R. J., C. Levesque, and S. K. Juniper. 2005. Biotic Interactions and Feedback Processes in Deep-Sea Hydrothermal Vent Ecosystems, p. 299–321. In E. Kristensen, R.R. Haese, and J.E. Kostka [eds.], Interactions Between Macro and Microorganisms in Marine Sediments. American Geophysical Union.
- Levin, S. A. 1992. The problem of pattern and scale in ecology. Robert H. MacArthur Award Lect. **73**: 1943–1967.
- Limén, H., C. J. Stevens, Z. Bourass, and S. K. Juniper. 2008. Trophic ecology of siphonostomatoid copepods at deep-sea hydrothermal vents in the northeast Pacific. Mar. Ecol. Prog. Ser. **359**: 161–170. doi:10.3354/meps07344
- Lutz, R. A., T. M. Shank, G. W. Luther, and others. 2008. Interrelationships Between Vent Fluid Chemistry, Temperature, Seismic Activity, and Biological Community Structure at a Mussel-Dominated, Deep-Sea Hydrothermal Vent Along the East Pacific Rise. J.

- Shellfish Res. **27**: 177–190. doi:10.2983/0730-8000(2008)27[177:ibvfct]2.0.co;2
- Mack, G. A., and J. H. Skillings. 1980. A Friedman-Type Rank Test for Main Effects in a Two Factor ANOVA. *J. Am. Stat. Assoc.* **75**: 947–951.
- Marcus, J., V. Tunnicliffe, and D. A. Butterfield. 2009. Post-eruption succession of macrofaunal communities at diffuse flow hydrothermal vents on Axial Volcano , Juan de Fuca Ridge , Northeast Pacific. *Deep. Res. Part II* **56**: 1586–1598.
doi:10.1016/j.dsr2.2009.05.004
- Marticorena, J., M. Matabos, E. Ramirez-Llodra, and others. 2021. Recovery of hydrothermal vent communities in response to an induced disturbance at the Lucky Strike vent field (Mid-Atlantic Ridge). *Mar. Environ. Res.* 105316. doi:10.1016/j.marenvres.2021.105316
- Martins, I., A. Colaço, P. R. Dando, I. Martins, D. Desbruyères, P. M. Sarradin, J. C. Marques, and R. Serrão-Santos. 2008. Size-dependent variations on the nutritional pathway of *Bathymodiolus azoricus* demonstrated by a C-flux model. *Ecol. Modell.* **217**: 59–71. doi:10.1016/j.ecolmodel.2008.05.008
- Martins, I., A. Colaço, R. S. Santos, F. Lesongeur, A. Godfroy, P. M. Sarradin, and R. P. Cosson. 2009. Relationship between the occurrence of filamentous bacteria on *Bathymodiolus azoricus* shell and the physiological and toxicological status of the vent mussel. *J. Exp. Mar. Bio. Ecol.* **376**: 1–6. doi:10.1016/j.jembe.2009.05.001
- Martins, I., R. P. Cosson, V. Riou, P. M. Sarradin, J. Sarrazin, R. S. Santos, and A. Colaço. 2011. Relationship between metal levels in the vent mussel *Bathymodiolus azoricus* and local microhabitat chemical characteristics of Eiffel Tower (Lucky Strike). *Deep. Res. Part I Oceanogr. Res. Pap.* **58**: 306–315. doi:10.1016/j.dsr.2011.01.002
- Mat, A., J. Sarrazin, G. Markov, and others. 2020. Biological rhythms in the deep-sea

- hydrothermal mussel *Bathymodiolus azoricus*. *Nat. Commun.* 1–12.
doi:10.1038/s41467-020-17284-4
- Matabos, M., and A. Arnaubec. 2015. Eiffel Tower hydrothermal chimney (Lucky Strike Hydrothermal Field, Mid Atlantic Ridge): 3D scene and imagery. SEANOE.
doi:https://doi.org/10.17882/79218
- Matabos, M., M. Best, J. Blandin, and others. 2016. Seafloor Observatories, p. 306–337. *In* M.R. Clark, M. Consalvey, and A.A. Rowden [eds.], *Biological Sampling in the Deep Sea*. John Wiley & Sons, Ltd.
- Matabos, M., D. Cuvelier, J. Brouard, and others. 2015. Behavioural study of two hydrothermal crustacean decapods: *Mirocaris fortunata* and *Segonzacia mesatlantica*, from the Lucky Strike vent field (Mid-Atlantic Ridge). *Deep. Res. Part II Top. Stud. Oceanogr.* **121**: 146–158. doi:10.1016/j.dsr2.2015.04.008
- McCook, L. J., and A. R. O. Chapman. 1997. Patterns and variations in natural succession following massive ice- scour of a rocky intertidal seashore. *J. Exp. Mar. Bio. Ecol.* **214**: 121–147. doi:10.1016/S0022-0981(96)02751-7
- McGrorty, S., and J. D. Goss-Custard. 1993. Population Dynamics of the Mussel *Mytilus edulis* along Environmental Gradients : Spatial Variations in Density-Dependent Mortalities. *J. Anim. Ecol.* **62**: 415–427.
- McMahon, B. R. 1988a. Physiological responses to oxygen depletion in intertidal animals. *Integr. Comp. Biol.* **28**: 39–53. doi:10.1093/icb/28.1.39
- McMahon, R. F. 1988b. Respiratory response to periodic emergence in intertidal molluscs. *Integr. Comp. Biol.* **28**: 97–114. doi:10.1093/icb/28.1.97
- Menge, B. A. 1978. Predation intensity in a rocky intertidal community - Relation between

- predator foraging activity and environmental harshness. *Oecologia* **34**: 1–16.
doi:10.1007/BF00346237
- Menge, B. A., and J. P. Sutherland. 1976. Species Diversity Gradients : Synthesis of the Roles of Predation, Competition, and Temporal Heterogeneity. *Am. Nat.* **110**: 351–369.
- Micheli, F., C. H. Peterson, L. S. Mullineaux, C. R. Fisher, S. W. Mills, G. Sancho, G. A. Johnson, and H. S. Lenihan. 2002. Predation structures communities at deep-sea hydrothermal vents. *Ecol. Monogr.* **72**: 365–382. doi:10.1890/0012-9615(2002)072[0365:PSCADS]2.0.CO;2
- Minchinton, T. E., R. E. Scheibling, and H. L. Hunt. 1997. Recovery of an intertidal assemblage following a rare occurrence of scouring by Sea Ice in Nova Scotia, Canada. *Bot. Mar.* **40**: 139–148. doi:10.1515/botm.1997.40.1-6.139
- Mittelstaedt, E., J. Escartín, N. Gracias, J. A. Olive, T. Barreyre, A. Davaille, M. Cannat, and R. Garcia. 2012. Quantifying diffuse and discrete venting at the Tour Eiffel vent site, Lucky Strike hydrothermal field. *Geochemistry, Geophys. Geosystems* **13**.
doi:10.1029/2011GC003991
- Mullineaux, L. S., C. H. Peterson, F. Micheli, and S. W. Mills. 2003. Successional mechanism varies along a gradient in hydrothermal fluid flux at deep-sea vents. *Ecol. Monogr.* **73**: 523–542. doi:10.1890/02-0674
- Nakamura, R. 1976. Temperature and the Vertical Distribution of Two Tidepool Fishes (*Oligocottus maculosus*, *O. snyderi*). *Am. Soc. Ichthyol. Herpetol.* 143–152.
- Nedoncelle, K., F. Lartaud, L. Contreira Pereira, M. Yücel, A. M. Thurnherr, L. Mullineaux, and N. Le Bris. 2015. Bathymodiolus growth dynamics in relation to environmental fluctuations in vent habitats. *Deep. Res. Part I Oceanogr. Res. Pap.* **106**: 183–193.

doi:10.1016/j.dsr.2015.10.003

Nedoncelle, K., F. Lartaud, M. de Rafelis, S. Boulila, and N. Le Bris. 2013. A new method for high-resolution bivalve growth rate studies in hydrothermal environments. *Mar. Biol.*

160: 1427–1439. doi:10.1007/s00227-013-2195-7

Nehls, G., I. Hertzler, and G. Scheiffarth. 1997. Stable mussel *Mytilus edulis* beds in the Wadden Sea - They're just for the birds. *Helgolander Meeresuntersuchungen* **51**: 361–372. doi:10.1007/BF02908720

Nehls, G., and M. Thiel. 1993. Large-scale distribution patterns of the mussel *Mytilus edulis* in the Wadden Sea of Schleswig-Holstein: Do storms structure the ecosystem?

Netherlands J. Sea Res. **31**: 181–187. doi:10.1016/0077-7579(93)90008-G

Newell, R. C. 1973. Factors affecting the respiration of intertidal invertebrates. *Integr. Comp. Biol.* **13**: 513–528. doi:10.1093/icb/13.2.513

Okamura, B. 1986. Group living and the effects of spatial position in aggregations of *Mytilus edulis*. *Oecologia* **69**: 341–347. doi:10.1007/BF00377054

Ondréas, H., M. Cannat, Y. Fouquet, A. Normand, P. M. Sarradin, and J. Sarrazin. 2009.

Recent volcanic events and the distribution of hydrothermal venting at the Lucky Strike hydrothermal field, Mid-Atlantic Ridge. *Geochemistry, Geophys. Geosystems* **10**.

doi:10.1029/2008GC002171

Paine, R. T. 1974. Intertidal community structure - Experimental studies on the relationship between a dominant competitor and its principal predator. *Oecologia* **15**: 93–120.

doi:10.1007/BF00345739

Paine, R. T. 1976. Size-Limited Predation : An Observational and Experimental Approach with the *Mytilus*- *Pisaster* Interaction. *Ecology* **57**: 858–873.

- Paine, R. T., and S. A. Levin. 1981. Intertidal Landscapes : Disturbance and the Dynamics of Pattern. *Ecol. Monogr.* **51**: 145–178. doi:<http://www.jstor.org/stable/2937261>
- Pester, N. J., E. P. Reeves, M. E. Rough, K. Ding, J. S. Seewald, and W. E. Seyfried. 2012. Subseafloor phase equilibria in high-temperature hydrothermal fluids of the Lucky Strike Seamount (Mid-Atlantic Ridge, 37°17'N). *Geochim. Cosmochim. Acta* **90**: 303–322. doi:10.1016/j.gca.2012.05.018
- Petratis, P. S. 1995. The Role of Growth in Maintaining Spatial Dominance by Mussels (*Mytilus Edulis*). *Ecology* **76**: 1337–1346.
- Pieters, H., J. H. Kluytmans, D. I. Zandee, and G. C. Cadée. 1980. Tissue composition and reproduction of *Mytilus edulis* en relation to food availability. *Netherlands J. Sea Res.* **14**: 349–361.
- Podowski, E. L., T. S. Moore, K. A. Zelnio, G. W. Luther, and C. R. Fisher. 2009. Distribution of diffuse flow megafauna in two sites on the Eastern Lau Spreading Center, Tonga. *Deep. Res. Part I Oceanogr. Res. Pap.* **56**: 2041–2056. doi:10.1016/j.dsr.2009.07.002
- Portail, M., C. Brandily, C. Cathalot, A. Colaço, Y. Gélinas, B. Husson, P. M. Sarradin, and J. Sarrazin. 2018. Food-web complexity across hydrothermal vents on the Azores triple junction. *Deep. Res. Part I Oceanogr. Res. Pap.* **131**: 101–120. doi:10.1016/j.dsr.2017.11.010
- Preisendorfer, R. W., and C. D. Mobley. 1988. Principal component analysis in meteorology and oceanography,.
- Pruis, M. J., and H. P. Johnson. 2004. Tapping into the sub-seafloor: Examining diffuse flow and temperature from an active seamount on the Juan de Fuca Ridge. *Earth Planet. Sci.*

Lett. **217**: 379–388. doi:10.1016/S0012-821X(03)00607-1

R Core Team. 2016. R: A language and environment for statistical computing.

Rasband, W. S. 1997. ImageJ.

Riou, V., A. Colaço, S. Bouillon, and others. 2010. Mixotrophy in the deep sea: A dual endosymbiotic hydrothermal mytilid assimilates dissolved and particulate organic matter. *Mar. Ecol. Prog. Ser.* **405**: 187–201. doi:10.3354/meps08515

Rosenberg, D. B., and S. M. Freedman. 1994. Temporal heterogeneity and ecological community structure. *Int. J. Environ. Stud.* **46**: 97–102.
doi:10.1080/00207239408710916

Rubio, I., U. Ganzedo, A. J. Hobday, and E. Ojea. 2020. Southward re-distribution of tropical tuna fisheries activity can be explained by technological and management change. *Fish Fish.* **21**: 511–521. doi:10.1111/faf.12443

Rybakova, E., and S. Galkin. 2015. Hydrothermal assemblages associated with different foundation species on the East Pacific Rise and Mid-Atlantic Ridge, with a special focus on mytilids. *Mar. Ecol.* **36**: 45–61. doi:10.1111/maec.12262

Sancho, G., C. R. Fisher, S. Mills, F. Micheli, G. A. Johnson, H. S. Lenihan, C. H. Peterson, and L. S. Mullineaux. 2005. Selective predation by the zoarcid fish *Thermarces cerberus* at hydrothermal vents. *Deep. Res. Part I Oceanogr. Res. Pap.* **52**: 837–844.
doi:10.1016/j.dsr.2004.12.002

Sarradin, P.-M., J.-C. Caprais, R. Riso, R. Kerouel, and A. Aminot. 1999. Chemical environment of the hydrothermal mussel communities in the Lucky Strike and Menez Gwen vent fields, Mid Atlantic Ridge. *Cah. Biol. Mar.* **40**: 93–104.

Sarrazin, J., J. Blandin, L. Delauney, and others. 2007. TEMPO: A new ecological module for

- studying deep-sea community dynamics at hydrothermal vents. *Ocean. 2007 - Eur.* 1–4.
doi:10.1109/oceanse.2007.4302310
- Sarrazin, J., D. Cuvelier, L. Peton, P. Legendre, and P.-M. Sarradin. 2014. High-resolution dynamics of a deep-sea hydrothermal mussel assemblage monitored by the EMSO-Açores MoMAR observatory. *Deep. Res. Part I Oceanogr. Res. Pap.* **90**: 62–75.
doi:10.1016/j.dsr.2014.04.004
- Sarrazin, J., and K. S. Juniper. 1998. The use of video imagery to gather biological information at deep-sea hydrothermal vents. *Cah. Biol. Mar.* **39**: 255–258.
- Sarrazin, J., and S. K. Juniper. 1999. Biological characteristics of a hydrothermal edifice mosaic community. *Mar. Ecol. Prog. Ser.* **185**: 1–19. doi:10.3354/meps185001
- Sarrazin, J., P. Legendre, F. de Busserolles, and others. 2015. Biodiversity patterns, environmental drivers and indicator species on a high-temperature hydrothermal edifice, Mid-Atlantic Ridge. *Deep. Res. Part II Trop. Stud. Oceanogr.* **121**: 177–192.
doi:10.1016/j.dsr2.2015.04.013
- Sarrazin, J., C. Levesque, S. K. Juniper, and M. K. Tivey. 2002. Mosaic community dynamics on Juan de Fuca Ridge sulphide edifices: Substratum, temperature and implications for trophic structure. *Cah. Biol. Mar.* **43**: 275–279. doi:10.21411/cbm.a.8e98c7cc
- Sarrazin, J., M. Portail, E. Legrand, C. Cathalot, A. Laes, N. Lahaye, P. M. Sarradin, and B. Husson. 2020. Endogenous versus exogenous factors: What matters for vent mussel communities? *Deep. Res. Part I* 103260. doi:10.1016/j.dsr.2020.103260
- Sarrazin, J., V. Robigou, S. K. Juniper, and J. R. Delaney. 1997. Biological and geological dynamics over four years on a high-temperature sulfide structure at the Juan de Fuca Ridge hydrothermal observatory. *Mar. Ecol. Prog. Ser.* **153**: 5–24.

doi:10.3354/meps153005

- Sarrazin, J., C. Walter, P. M. Sarradin, and others. 2006. Community structure and temperature dynamics within a mussel assemblage on the Southern East Pacific Rise. *Cah. Biol. Mar.* **47**: 483–490. doi:10.21411/cbm.a.3e05e5ec
- Scheirer, D. S., T. M. Shank, and D. J. Fornari. 2006. Temperature variations at diffuse and focused flow hydrothermal vent sites along the northern East Pacific Rise. *Geochemistry, Geophys. Geosystems* **7**. doi:10.1029/2005GC001094
- Schoening, T., J. Osterloff, and T. W. Nattkemper. 2016. RecoMIA-recommendations for marine image annotation: Lessons learned and future directions. *Front. Mar. Sci.* **3**. doi:10.3389/fmars.2016.00059
- Sen, A., S. Kim, A. J. Miller, K. J. Hovey, S. Hourdez, G. W. Luther, and C. R. Fisher. 2016. Peripheral communities of the Eastern Lau Spreading Center and Valu Fa Ridge: community composition, temporal change and comparison to near-vent communities. *Mar. Ecol.* **37**: 599–617. doi:10.1111/maec.12313
- Sen, A., E. L. Podowski, E. L. Becker, and others. 2014. Community succession in hydrothermal vent habitats of the Eastern Lau Spreading Center and Valu Fa Ridge, Tonga. *Limnol. Oceanogr.* **59**: 1510–1528. doi:10.4319/lo.2014.59.5.1510
- Shank, T., D. Fornari, D. . Yoerger, and others. 2003. Deep Submergence Synergy: Alvin and ABE Explore the Galapagos Rift at 86°W. *Eos (Washington, DC)*. **84**: 425–440.
- Shank, T. M., D. J. Fornari, K. L. Von Damm, M. D. Lilley, R. M. Haymon, and R. A. Lutz. 1998. Temporal and spatial patterns of biological community development at nascent deep-sea hydrothermal vents (9°50'N, East Pacific Rise). *Deep. Res. Part II Top. Stud. Oceanogr.* **45**: 465–515. doi:10.1016/S0967-0645(97)00089-1

- Singh, S. C., W. C. Crawford, H. Carton, and others. 2006. Discovery of a magma chamber and faults beneath a Mid-Atlantic Ridge hydrothermal field. *Nature* **442**: 1029–1032.
doi:10.1038/nature05105
- Sousa, W. P. 1979. Disturbance in Marine Intertidal Boulder Fields : The Nonequilibrium Maintenance of Species Diversity. *Ecology* **60**: 1225–1239.
- Sousa, W. P. 1984. Intertidal Mosaics : Patch Size, Propagule Availability, and Spatially Variable Patterns of Succession. *Ecology* **65**: 1918–1935.
- Steenbergen, J., J. M. D. D. Baars, M. R. Van Stralen, and J. A. Craeymeersch. 2006. Winter survival of mussel beds in the intertidal part of the Dutch Wadden Sea. *NERI Tech. Rep.* 107–111.
- Strasser, M., T. Reinwald, and T. Reise. 2001. Differential effects of the severe winter of 1995/96 on the intertidal bivalves *Mytilus edulis*, *Cerastoderma edule* and *Mya arenaria* in the Northern Wadden Sea. *Helgol. Mar. Res.* **55**: 190–197.
doi:10.1007/s101520100079
- Suchanek, T. H. 1978. The ecology of *Mytilus edulis* L. in exposed rocky intertidal communities. *J. Exp. Mar. Bio. Ecol.* **31**: 105–120. doi:10.1016/0022-0981(78)90139-9
- Suchanek, T. H. 1981. The role of disturbance in the evolution of life history strategies in the intertidal mussels *Mytilus edulis* and *Mytilus californianus*. *Oecologia* **50**: 143–152.
doi:10.1007/BF00348028
- Taylor, C. D., C. O. Wirsén, and F. Gaill. 1999. Rapid microbial production of filamentous sulfur mats at hydrothermal vents. *Appl. Environ. Microbiol.* **65**: 2253–2255.
doi:10.1128/aem.65.5.2253-2255.1999
- Tivey, M. K. 2007. Generation of Seafloor Hydrothermal Vent Fluids and Associated Mineral

- Deposits. *Oceanography* **20**: 50–65.
- Tsuchiya, M. 1983. Mass mortality in a population of the mussel *Mytilus edulis* L. Caused by high temperature on rocky shores. *J. Exp. Mar. Bio. Ecol.* **66**: 101–111.
doi:10.1016/0022-0981(83)90032-1
- Tsurumi, M., and V. Tunnicliffe. 2003. Tubeworm-associated communities at hydrothermal vents on the Juan de Fuca Ridge , northeast Pacific. *Deep. Res. I* **50**: 611–629.
doi:10.1016/S0967-0637(03)00039-6
- Tunnicliffe, V. 1990. Observations on the Effects of Sampling on Hydrothermal Vent Habitat and Fauna of Axial Seamount , Juan de Fuca Ridge. *J. Geophys. Res.* **95**: 12961–12966.
- Tunnicliffe, V. 1991. The biology of hydrothermal vents: ecology and evolution., p. 319–407. *In* H. Barnes, M. Barnes, A.D. Ansell, and R.N. Gibson [eds.], *Oceanography and Marine Biology Annual Review*.
- Tunnicliffe, V., J. F. Garrett, and H. Paul Johnson. 1990. Physical and biological factors affecting the behaviour and mortality of hydrothermal vent tubeworms (vestimentiferans). *Deep. Res.* **37**: 103–125.
- Tunnicliffe, V., J. F. Holden, D. A. Butterfield, and S. K. Juniper. 1997. Biological colonization of new hydrothermal vents following an eruption on Juan de Fuca Ridge. *Deep. Res. I* **44**: 1627–1644.
- Tunnicliffe, V., and K. S. Juniper. 1990. Dynamic character of the hydrothermal vent habitat and the nature of sulphide chimney fauna. *Prog. Oceanogr.* **24**: 1–13. doi:10.1016/0079-6611(90)90015-T
- Tyler, P. A., and C. M. Young. 1999. Reproduction and dispersal at vents and cold seeps. *J. Mar. Biol. Assoc. United Kingdom* **79**: 193–208. doi:10.1017/S0025315499000235

- Underwood, N., P. Hambäck, and B. D. Inouye. 2005. Large-scale questions and small-scale data: Empirical and theoretical methods for scaling up in ecology. *Oecologia* **145**: 177–178. doi:10.1007/s00442-005-0057-9
- Urcuyo, I. A., G. J. Massoth, D. Julian, and C. R. Fisher. 2003. Habitat, growth and physiological ecology of a basaltic community of *Ridgeia piscesae* from the Juan de Fuca Ridge. *Deep. Res. Part I Oceanogr. Res. Pap.* **50**: 763–780. doi:10.1016/S0967-0637(03)00061-X
- Vismann, B. 1991. Sulfide tolerance: physiological mechanisms and ecological implications. *Ophelia* **34**: 1–27. doi:10.1080/00785326.1991.10429703
- Vohsen, S. A., H. R. Gruber-Vodicka, E. O. Osman, M. A. Saxton, S. B. Joye, N. Dubilier, C. R. Fisher, and I. B. Baums. 2020. Deep-sea corals near cold seeps associate with chemoautotrophic bacteria that are related to the symbionts of cold seep and hydrothermal vent mussels. bioRxiv.
- Vuillemin, R., D. Le Roux, P. Dorval, K. Bucas, J. P. Sudreau, M. Hamon, C. Le Gall, and P. M. Sarradin. 2009. CHEMINI: A new in situ CHEMical MINIaturized analyzer. *Deep. Res. Part I Oceanogr. Res. Pap.* **56**: 1391–1399. doi:10.1016/j.dsr.2009.02.002
- Wiens, J. A., N. C. Stenseth, B. Van Horne, and R. A. Ims. 1993. Ecological Mechanisms and Landscape Ecology. *Oikos* **66**: 369–380.
- Wilson, J. H., and R. Seed. 1974. Reproduction in *Mytilus edulis* L. (Mollusca: Bivalvia) in Carlingford Lough, Northern Ireland. *Irish Fish. Investig.* **15**: 31.
- Witman, J. D. 1987. Subtidal Coexistence : Storms , Grazing , Mutualism , and the Zonation of Kelps and Mussels. *Ecol. Monogr.* **57**: 167–187.
- Woodin, S. A. 1974. Adult-larval interactions in dense infaunal assemblages: patterns of

abundance. *J. Mar. Res.* **44**: 171–187.

Wootton, J. T. 1993. Size-Dependent Competition: Effects on the Dynamics Vs. The End Point of Mussel Bed Succession. *Ecology* **74**: 195–206.

Wootton, J. T. 2001. Local interactions predict large-scale pattern in empirically derived cellular automata. *Nature* **413**: 841–844. doi:10.1038/35101595

Zajac, R. N., R. B. Whitlatch, and S. F. Thrush. 1998. Recolonization and succession in soft-sediment infaunal communities: The spatial scale of controlling factors. *Hydrobiologia* **375–376**: 227–240. doi:10.1007/978-94-017-2864-5_19

Table 2 – Results of least-square linear regressions applied on periods of mussel total cover recorded in two fields of view (FoVs) (Figure 3A & 3B). Only slope values are given with their associated adjusted R², degrees of freedom (df) and F-statistics. Significant slopes are indicated with asterisks (*p*-value: * < 0.05, ** < 0.01, *** < 0.001). ¹Only 6 months of data from 30 July 2017 to 19 January 2018 and from 29 September 2018 to 30 March 2019.

FoV	Period	Slope [dm ² /month]	Adjusted R ²	df	F-statistic
2012-2015	2012-2013	+ 0.19***	0.74	12	36.85
	2013-2014	+ 0.10	- 0.15	3	0.46
	2014-2015	- 0.03	- 0.11	8	0.14
2012-2019	2012-2013	+ 0.10***	0.66	12	26.20
	2013-2014	+ 0.10	0.00	3	1.01
	2014-2015	+ 0.03	- 0.05	8	0.54
	2015-2016	+ 0.11***	0.72	12	34.58
	2016-2017	- 0.06	-0.21	3	0.30
	2017-2018	- 0.10	0.35	6	4.75
	2018-2019	- 0.16	0.82	9	46.24
	2017-2018 ¹	- 0.27**	0.84	5	31.75
	2018-2019 ¹	- 0.26***	0.92	5	73.83

Table 3 – Environmental factors measured in the TEMPO ecological observation module (EMSO-Azores observatory) field of view: (A) Yearly submersible measurements (n = 116) of temperature for 1 minute (n = 87) and CHEMINI analysers (dissolved Fe(II) [n = 77] and total sulphide concentrations [n = 99]) from 2014 to 2019. (B) iButton® probe temperatures repositioned monthly by annotating their position in TEMPO images from 2014 to 2019. Average temperatures using continuous recordings were retrieved automatically using a temporal window of 1 week (± 0.5 °C) (n = 21,988). The maximum weekly average temperature is also given. Measurements were assigned to substratum and taxa based on the visual position of the submersible probes during dives (A) or considering a buffer zone with a radius of 5 cm around the iButton® probes (B). When iButton® temperature sensors were not linked to any particular substratum/taxon, temperature was assigned to the “no cover” class, i.e. the slab substratum. Classes (i.e. columns) are arranged according to the empirical distance of biological features (assemblage type or dominant taxon) and substrata to the vent orifice commonly observed at the hydrothermal edifice Eiffel Tower (Lucky Strike vent field; Cuvelier et al., 2009; Girard et al., 2020). Arrows indicate this theoretical gradient of the fluid dilution. No standard deviation refers to single point measurements.

Environmental factor		← ← ← ← ←					Hydrothermal vent orifice	→ Farthest from the vent orifice	
		Biological features						Substratum	
		Zoanthids	Microbial mat	Sparse <i>Bathymodiolus azoricus</i> assemblage	Dense <i>Bathymodiolus azoricus</i> assemblage	<i>Segonzacia mesatlantica</i>	Close vicinity to the vent orifice	White material	Slab substratum
(A) Data collected during submersible dives	Mean temperature \pm SD [°C]	5.1	No data	5.0 \pm 0.1	6.2 \pm 1.5	No data	39.1 \pm 36.4	5.8 \pm 0.4	4.9 \pm 0.4
	Mean Fe concentration \pm SD [μ mol/L]	0.4	1.6	1.2 \pm 2.9	1.1 \pm 1.2	No data	9.0 \pm 14.2	0.3 \pm 0.5	1.3 \pm 2.2
	Mean sulphur concentration \pm SD [μ mol/L]	7.4 \pm 9.0	15.4	5.0 \pm 7.9	19.0 \pm 28.0	No data	107.2 \pm 105.8	12.0 \pm 13.9	10.9 \pm 25.7
(B) Data collected via iButton® probes	Mean temperature \pm SD [°C]	No data	5.8 \pm 0.2	(no distinction made in cover type) 6.8 \pm 3.2		9.8 \pm 6.0	No data	9.5 \pm 5.2	6.2 \pm 1.6
	Maximum temperature [°C]	No data	6.0		25.1	23.8	No data	25.1	12.7

Table 4 – Abiotic and biotic conditions affecting the dynamics of mussel assemblages in the intertidal and hydrothermal environments. Not affected (-), affected (+; behavioural response, influence on few individuals only), strongly affected (++; > decimetre-scale influence in assemblages).

Source of influence	Process involved	Effect	
		Intertidal	Hydrothermal
Environmental			
<i>Infra-daily</i>			
Tides	Predictable changes	++	+
	Hydrodynamics & tidal variation	Desiccation/Temperature stress¹ 11, 22, 38, 43 Physical disturbance (log/boulder drift, waves)^{2, 3, 18, 21, 28, 56}	Changes in the distribution of the hydrothermal fluid carrying stressors and trophic resources 23, 65, 66, 61, 70, 72
<i>Infra-annual</i>			
Substratum instability		Little investigated	++ Structural collapse^{23, 36} Activation/deactivation of fluid outflow^{36, 60, 67}
Season	Storms	++	+
	Disturbance on hydrodynamics	Water velocity^{3, 13, 16, 18, 25, 26, 40}	Bottom pressure, current velocity^{24, 30, 70}
	Climate extremes	++	-
	Disturbance linked to winter ice and high/low temperatures	Physical dislodgement (e.g. ice scouring) and/or extreme environmental conditions 11, 17, 18, 33, 34, 44, 52, 53	Our data suggest high stability of the background deep-sea environment

Life-history trait		+	+
Spawning induction		<i>Mytilus edulis</i> spawns seasonally ⁷ , 15, 31 <i>Mytilus californianus</i> : spawns continuously ¹²	Seasonal spawning of all species of <i>Bathymodiolus</i> ^{42, 50, 51} except <i>B.</i> <i>thermophilus</i> ⁷¹
<i>Decadal and more</i>			
Magmatic event	Eruption, earthquake	-	++
		<i>Not necessarily an intertidal feature. Few cases with mortality</i> ⁵⁷	<i>Fauna removal at medium to fast- spreading ridges</i> ⁵⁹
Long-term habitat change	Habitat suitability decline	++ Sanding up ⁵⁸	++ Waning ^{47, 62, 67, 68} Landslide ³⁶
Biotic			
Predation		++	-/+
		Interspecific ^{3, 6, 9, 10, 11, 16, 27, 29, 32, 35, 39, 40}	Interspecific ^{45, 48, 49, 69, 63, 73} Larviphagy ⁵⁴
Competition for space/resources		++ Interspecific ^{1, 3, 4, 5, 9, 11} Intraspecific ^{19, 27}	++ Interspecific ^{36, 41, 55, 67}
Recolonisation		++ Recruitment ^{27, 64} Passive/active displacement ^{16, 27}	++ Recruitment ^{37, 41} Active displacement ^{67, 69}

Connell 1. 1961, 2. 1985; 3. Dayton 1971; 4. Harger 1972; Paine 5. 1974, 6. 1976; 7. Wilson and Seed 1974; 8. Woodin 1974; 9. Menge and Sutherland 1976; 10. Menge 1978; Suchanek 11. 1978, 12. 1981; Sousa 13. 1979, 14. 1984; 15. Pieters et al. 1980; 16. Paine and Levin 1981; 17. Tsuchiya 1983; 18. Dethier 1984; 19. Bertness and Grosholz 1985; 20. Okamura 1986; 21. Denny 1987; 22. McMahon 1988b; 23. Tunnicliffe and Juniper 1990; 24. Cannon et al. 1991; 25. McGrorty and Goss-Custard 1993; 26. Nehls and Thiel 1993; Wootton 27. 1993, 28. 2001; 29. Petraitis 1995; 30. Cannon and Thomson 1996; 31. Gray et al. 1997; 32. Hilgerloh et al. 1997; 33. McCook and Chapman 1997; 34. Minchinton et al. 1997; 35. Nehls et al. 1997;

36. Sarrazin et al. 1997; 37. Comtet and Desbruyeres 1998; 38. Denny and Paine 1998; Hunt and Scheibling 39. 1998, 40. 2001; 41. Shank et al. 1998; 42. review in Tyler and Young 1999; 43. Denny and Wethey 2001; 44. Strasser et al. 2001; 45. Micheli et al. 2002; 46. Mullineaux et al. 2003; 47. Tsurumi and Tunnicliffe 2003; 48. Urcuyo et al. 2003; 49. Sancho et al. 2005; 50. Colaço et al. 2006; 51. Dixon et al. 2006; 52. Steenbergen et al. 2006; 53. Beukema and Dekker 2007; 54. Lenihan et al. 2008; 55. Lutz et al. 2008; 56. van De Koppel et al. 2008; 57. Castilla et al. 2010; 58. Dolch and Reise 2010; 59. review in Glover et al. 2010; Cuvelier et al. 60. 2011b, 61. 2014; 62. Fabri et al. 2011; 63. Govenar 2012; 64. Khaitov 2013; Nedoncelle et al. 65. 2013, 66. 2015; Sen et al. 67. 2014, 68. 2016; 69. Matabos et al. 2015; 70. Lelièvre et al. 2017; 71. review in Laming et al. 2018; 72. Mat et al. 2020; 73. Marticorena et al. 2021

The authors declare that the research was conducted in the absence of any commercial or financial relationships that could be construed as a potential conflict of interest.

- The diffuse-flow habitat was highly stable over 7 years
- The *Bathymodiolus azoricus* mussel assemblage was remarkably stable over 7 years
- Microbial mats displayed heterogeneous spatio-temporal dynamics
- The zoanthid assemblage was highly stable
- Few biotic interactions were observed such as facilitation mechanisms
- Comparison to intertidal mussel dynamics demonstrates a regime of infrequent disturbance on vent assemblages